A brainstem to hypothalamic arcuate nucleus GABAergic circuit drives feeding

Pablo B Martinez de Morentin[†*1,2], J Antonio Gonzalez[1], Georgina K.C. Dowsett[3], Yuliia Martynova[1], Giles S.H. Yeo[3], Sergiy Sylantyev[*1], Lora K Heisler[1]

[1]The Rowett Institute, University of Aberdeen, UK.

[2]School of Biomedical Sciences, Faculty of Biological Sciences, University of Leeds, UK

[3]MRC Metabolic Diseases Unit, Wellcome-MRC Institute of Metabolic Science, Addenbrooke's Hospital, University of Cambridge, CB2 0QQ, United Kingdom.

[†]Lead author

*Correspondence

p.demorentin@leeds.ac.uk

s.sylantyev@abdn.ac.uk

ORCIDs:

PBM 0000-0002-0684-3215

JAG 0000-0001-7045-4831

GKCD 0000-0002-2134-8554

YM 0000-0003-1927-3298

GSHY 0000-0001-8823-3615

SS 0000-0002-1358-0601

LKH 0000-0002-7731-1419

Highlights

- Nucleus of the solitary tract (NTS) GABA neurons are responsive to nutritional status.
- Chemogenetic $GABA^{NTS}$ neuron activation reduces food intake and body weight.
- $GABA^{NTS}$ projections to the hypothalamic arcuate nucleus (ARC) promote satiety.
- Optogenetic $GABA^{NTS}$→ARC stimulation inhibits orexigenic AgRP/NPY neurons.

In Brief

Martinez de Morentin et al. identify GABAergic neurons in the nucleus of the solitary tract as a new player in the circuit governing feeding behavior and body weight.

Abstract

The obesity epidemic is principally driven by the consumption of more calories than the body requires. It is therefore essential that the mechanisms underpinning feeding behavior are defined. The brainstem nucleus of the solitary tract (NTS) receives direct information from the digestive system and projects to second order regions in the brain. Though γ-Aminobutyric acid is widely expressed in the NTS ($GABA^{NTS}$), its function has not been defined. Characterization of GABA cells using single nucleus RNA sequencing (Nuc-Seq) identified at least 19 clusters. Here we provide insight into the function of $GABA^{NTS}$ cells, revealing that selective activation of $GABA^{NTS}$ neurons significantly controls food intake and body weight. Optogenetic interrogation of $GABA^{NTS}$ circuitry identified $GABA^{NTS}$→arcuate nucleus of the hypothalamus (ARC) projections as appetite suppressive without creating aversion. Electrophysiological analysis revealed $GABA^{NTS}$→ARC stimulation inhibits hunger promoting agouti-related protein/neuropeptide Y (AgRP/NPY) neurons via GABA release. Adopting an intersectional genetics strategy, we clarify that the $GABA^{NTS}$→ARC circuit induces satiety. These data identify $GABA^{NTS}$ as a new modulator of feeding behavior, body weight and controller of orexigenic AgRP/NPY activity, thereby providing insight into the neural underpinnings of obesity.

Keywords

y-Aminobutyric acid, agouti-related -peptide, Neuropeptide Y, nucleus of the solitary tract, food intake.

Introduction

Obesity represents a key challenge to human health and is primarily due to the consumption of calories in excess to body's energy requirements. Eating is a complex behavior that not only depends on the basic energy demands at a cellular and organism level, but also the integration of internal and environmental cues, the reward value of food, motivation, and conditioning behavior (Andermann & Lowell, 2017; Campos et al., 2022). The aim of the present study was to probe neurocircuitry regulating feeding and body weight with the objective of uncovering critical energy homeostasis circuitry.

One of the primary nodes for the integration of energy-related information from the periphery to the brain is the nucleus of the solitary tract (NTS) within the brainstem dorsal vagal complex (DVC)(Hyun & Sohn, 2022). The NTS contains a heterogeneous population of energy-related sensitive cells(Cheng et al., 2022; Dowsett et al., 2021; Grill & Hayes, 2012). Recent studies using single-nucleus RNA sequencing provide a detailed expression map of identified cellular populations involved in energy balance, and most were revealed to be glutamatergic(Dowsett et al., 2021; Ludwig et al., 2021). For example, subpopulations of these glutamatergic cells influencing energy balance include leptin receptor (LEPR)(Cheng et al., 2020), calcitonin receptor (CALCR)(J. Chen et al., 2020a), glucagon-like peptide 1 receptor (GLP-1R)(Alhadeff et al., 2017; Fortin et al., 2020), preproglucagon (PPG)(Holt et al., 2019), tyrosine hydroxylase (TH) (Aklan et al., 2020; J. Chen et al., 2020b), cholecystokinin (CCK) (D'Agostino et al., 2016) and proopiomelanocortin (POMC) (Georgescu et al., 2020; Zhan et al., 2013). However, very little is known about the role of NTS inhibitory GABA-releasing clusters ($GABA^{NTS}$) in energy homeostasis. One report in rats indicated a subpopulation of GLP-1R-expressing neurons releasing GABA are necessary mediators for the anorectic effects of the obesity medication liraglutide (Fortin et al., 2020). Therefore, $GABA^{NTS}$ represents and intriguing and understudied population of NTS cells and is the focus of the present study.

In the regulation of feeding behavior, one of the most widely studied projections from the NTS is to the hypothalamus (Aklan et al., 2020; Blevins et al., 2004; D'Agostino et al., 2016; Liu et al., 2017; Shi et al., 2021; Tsang et al., 2020). However, whether the arcuate nucleus of the hypothalamus (ARC) receives GABAergic inhibitory control from the NTS is not known. Within the ARC is a subpopulation of potent orexigenic neurons expressing both agouti-related peptide and neuropeptide Y (AgRP/NPY) (Betley et al., 2013; Hahn et al., 1998;

Heisler et al., 2006; Heisler & Lam, 2017). We hypothesized that GABA^{NTS} neurons significantly regulate feeding and body weight and project to and inhibit key hunger-stimulating AgRP/NPY cells.

Results

GABA^{NTS} cells are sensitive to energy status and modulate food intake

To characterize GABA^{NTS} neurons, we initially used a single nucleus RNA sequencing (NucSeq) dataset of the mouse dorsal vagal complex (Dowsett et al., 2021). Neuronal cells expressing transcripts for *Slc32a1* (solute carrier family 32 member 1 or vesicular GABA transporter, Vgat) were extracted and re-clustered, consisting of 1847 neurons, which formed 19 clusters (**Figure 1A**). Of these clusters, 2-Cacna2d1/Tmem163 expressed Vglut2 transcripts, and lower levels of *Gad1* and *Gad2.* Low expression of classical neurotransmitter related genes was found in these GABAergic neuronal clusters (**Figure 1B**). Adipocyte hormone Leptin receptor (*Lepr)* expression was identified in 13-Onecut2/Lepr and 15-Ebf2/Acly clusters (**Figure 1B**). We identified some expression of incretin receptors including glucagon-like receptor 1 (GLP-1R) and gastric inhibitory polypeptide receptor (GIPR) in several clusters (**Figure S1A**). Differential gene expression analysis was performed on each cluster to identify the effects of an overnight fast on transcript expression in GABAergic (*Slc32a1*+) neurons (**Figure S1B**). Cluster 3-Dcc/Cdh8 displayed significant upregulation in transcript expression in response to a fast, however 93.7% of this cluster originates from *ad libitum* fed animals. Significantly differentially regulated genes in *Slc32a1*$^{+}$ neurons can be found in **Figure S1C**. These data indicate minimal overlap with specific populations of NTS neurons that have been previously described with regards to energy balance.

We therefore, examined whether GABA^{NTS} cells are responsive to energy status. We facilitated the visualization of GABA^{NTS} neurons by crossing *Vgat-ires-Cre* mice with *tdTomato$^{fl/fl}$* reporter mice (*Vgat^{tdTom},* **Figure 1D and 1E**). We then examined the expression levels of the neuronal activity marker c-Fos (Olson et al., 1993) in mice that were overnight fasted and in mice that were refed for 2 hours after overnight fasting. Re-fed mice showed significantly more c-Fos in the NTS (**Figure S1D**) and specifically an increased number of GABAergic cells activated (**Figure 1F and 1G**) when compared to fasted mice. This suggests that GABA^{NTS} cells are responsive to positive energy status.

To determine whether GABA^{NTS} neurons have a role in the control of food intake, we used chemogenetic Designer Receptors Exclusively Activated by Designer Drugs (DREADD) to manipulate GABA^{NTS} cellular activity (Alexander et al., 2009). Specifically, AAVs expressing hM3Dq, hM4Di or control mCherry were bilaterally injected into the NTS of *Vgat*^{Cre} mice (**Figure 1H**). This allowed to modulate GABA^{NTS} neuron activity with the administration of the designer drug clozapine-N-oxide (CNO). Administration of CNO in hM3Dq-injected mice induced strong c-Fos expression in the NTS (**Figure 1I**). We next assessed the effect of the modulation of GABA^{NTS} on food intake in mice under different scenarios. In ad libitum fed mice, hM3Dq chemogenetic activation of GABA^{NTS} cells significantly reduced overall food intake during the active dark cycle when compared to control (mCherry) siblings (**Figure 1J and S1E**). Similarly, hM3Dq GABA^{NTS} cell activation reduced food intake in hunger-induced fasted mice when compared to control mice (**Figure S1F and S1G**). Conversely, hM4Di chemogenetic inhibition of GABA^{NTS} cell in satiated mice during the light cycle significantly increased food intake when compared to satiated littermate mCherry controls (**Figure 1K**).

Given the potent reduction of food intake produced by the activation of GABA^{NTS} neurons, we examined whether prolonged activation impacted body weight. Twice-daily administration of CNO (**Figure 1L)** in hM3Dq-expressing mice induced a significant reduction in daily food intake (**Figure 1M**) and a progressive reduction in body weight (**Figure 1N and 1O**). Although feeding returned to baseline levels 72 hours after the final CNO administration, body weight remained significantly lower in hM3Dq-expressing mice (**Figure 1N**). In contrast, prolonged GABA^{NTS} neuron inhibition using hM4Di did not induce greater food intake (**Figure S1H**) nor changes in body weight (**Figure S1I**) when compared to their littermate mCherry controls. These results indicate that the selective activation of GABA^{NTS} neurons is sufficient to result in a sustained reduction in energy intake and hence body weight.

Recently, it has been reported that the inhibition of neurons expressing the GABA-producing enzyme, glutamate decarboxylase (GAD), in the NTS of rats partially blunted the anorectic effect of the GLP1-R agonist liraglutide (Fortin et al., 2020). These data, suggest that GABA^{NTS} contributes to the therapeutic effects of GLP1-R agonists in rats. However, GLP-1R expression in rats and mice differs, especially its receptor density (Cork et al., 2015; Graham et al., 2020; Jensen et al., 2018). We therefore assessed the feeding response of liraglutide in GABA^{NTS}-hM4Di/mCherry-expressing mice. Chemogenetic inhibition of GABA^{NTS} partially blunted the acute anorectic effects of liraglutide (**Figure S1J and S1K**). This provides support that GABA^{NTS} participates in the anorectic effects of liraglutide in mice.

153

154 *Optogenetic stimulation of GABA^{NTS} terminals inhibits AgRP/NPY^{ARC} cells*

155 To clarify the circuitry through which GABA^{NTS} neurons influence feeding and body weight,
156 we used Channelrhodopsin 2 (ChR2)-assisted circuit mapping (CRACM) (González et al.,
157 2016; Petreanu et al., 2007). Specifically, an AAV expressing ChR2-mCherry was injected
158 into the NTS of *Vgat^{Cre}* mice (**Figure 2A**) and projection patterns were analyzed. GABA^{NTS}
159 cells project to hypothalamic subregions including the ARC, paraventricular nucleus (PVH)
160 and dorsomedial nucleus (DMH) and various other extra-hypothalamic regions (**Figure S2A**).
161 Within the ARC, we observed a dense array of projections (**Figure 2B**). This identified the
162 ARC as a candidate second order region involved in the GABA^{NTS} control of food intake and
163 body weight.

164 Fasting induces activation of AgRP/NPY-expressing neurons (Hahn et al., 1998) and direct
165 AgRP/NPY neuron activation induces robust feeding (Aponte et al., 2011; Krashes et al.,
166 2011). Since GABA-releasing neurons are the main inhibitory network in the brain (Krnjević
167 & Schwartz, 1967), we hypothesized that GABA^{NTS} cells projecting to the ARC would target
168 AgRP/NPY neurons to decrease food intake. To interrogate this potential
169 GABA^{NTS}→AgRP/NPY^{ARC} circuit, *Vgat^{Cre}* were crossed with *Npy^{hrGFP}* mice (*Vgat^{Cre}::Npy^{hrGFP}*)
170 and bilaterally injected with AAV-ChR2-mCherry into the NTS. We observed that a subset of
171 NPY^{hrGFP} cell bodies were surrounded by mCherry-containing fibers (**Figure 2C**). In contrast,
172 terminals were not found surrounding neurons expressing other neuropeptides involved in
173 the regulation of food intake such as POMC neurons (Williams & Schwartz, 2005) (**Figure**
174 **2D**).

175 We next investigated whether this anatomical connectivity produced functional interactions
176 between GABA^{NTS} terminals and AgRP/NPY^{ARC} and POMC neurons. Specifically, photo-
177 stimulation of ChR2-containing axon terminals from GABA^{NTS} neurons produced robust
178 synaptic responses in 14% of AgRP/NPY cells in the ARC but not in POMC cells (**Figure**
179 **2E**). The rapid synaptic currents triggered in AgRP/NPY cells by the optical stimulation
180 changed polarity near the equilibrium potential for chloride (**Figure 2F and 2G**), as expected
181 from ionotropic GABA receptors. Light-induced currents were unexpectedly small, and their
182 reversal potential was more positive than that expected for GABA-activated currents (about
183 -60 mV) (**Figure 2H-J**). These effects could be explained by voltage- and space-clamp errors
184 (Spruston et al., 1993) and in turn suggest that perhaps GABA^{NTS} terminals reach ARC NPY

cells at dendrites distant from the soma. While it is not possible to directly demonstrate that this is the case, we tested whether this reasoning was justified by simulating the optogenetic activation of GABA synaptic events at distal vs proximal dendrites in a model neuron. Using a predictive neuronal model (Lindroos & Hellgren Kotaleski, 2021), we found that GABAergic post-synaptic currents become progressively smaller with their reversal potential progressively more positive, the further the GABA inputs are from the soma (**Figure S2 B-E**).

Next, we tested whether activation of GABA receptors at NPY cells is accompanied by release of GABA from $GABA^{NTS}$ ChR2-containing terminals. We first stimulated ChR2-mCherry expressing $GABA^{NTS}$ fibers in the ARC and performed a "sniffer patch" experiment registering $GABA_AR$ single-channel openings above the NPY^{hrGFP} cells contacted by $GABA^{NTS}$ fibers (**Figure 2K**). In this experiment, the $GABA_AR$ response was isolated with a specific cocktail of antagonists (see Methods). This provides semi-quantitative monitoring of extracellular levels of GABA (Sylantyev et al., 2020). A burst of light directed to $GABA^{NTS}$ ChR2-containing terminals in the ARC induced single-channel openings in membrane patch in control conditions, and the currents had amplitudes comparable to GABAergic inhibitory currents (Sylantyev et al., 2020) (**Figure 2L, *left***). Application of $GABA_AR$ competitive antagonist gabazine reversibly blocked the single-channel openings (**Figure 2L, *middle and right***). The same pattern of receptor opening time was observed in all assessed patches (**Figure 2M**). This suggested that postsynaptic NPY cells are sensitive to $GABA^{NTS}$ presynaptic release of GABA.

To test whether NPY cells were inhibited by the release of GABA from $GABA^{NTS}$ terminals, we designed a protocol of additive subthreshold electrical stimuli. This method is designed to evoke an action potential after 5 stimuli. In addition, we coupled a 470 nm light burst to the same trigger (**Figure S2F**). We then alternated a sequence of electrical stimuli and electrical stimuli with light burst. The electrical stimulation evoked an action potential(s) (**Figure S2G, *left***) followed by low-frequency or no single-channel openings in the sniffer patch. When we coupled the electrical stimulation with the light burst, the occurrence of actions potentials was blocked and accompanied with single-channel openings in a sniffer patch (**Figure S2G, *right***). This happened in all cells patched (**Figure S2H**). These openings resembled $GABA_AR$ openings illustrated in Figure 2L. Subsequent stimulations showed a decrease in channel opening intensity, suggesting a depletion of GABA stores from the presynaptic terminal, which was eventually insufficient to prevent the action potential (**Figure S2I**). These results

provide strong evidence that GABA^{NTS} fibers inhibit AgRP/NPY cells due to the release of the fast neurotransmitter GABA.

GABA^{NTS}→ARC optogenetic stimulation reduces feeding and is not aversive

Given the dense fiber projection pattern of NTS-GABAergic cells to the ARC, and that its activation induced a strong inhibition of AgRP/NPY neurons, we interrogated whether this circuit is sufficient to influence food intake. To investigate this, AAVs expressing ChR2-mCherry were infused into the NTS of *Vgat^{Cre}* mice and an optic fiber was placed above the ARC (**Figure 3A**). Food intake was measured both without and with ARC photo-stimulation prior to the onset of the dark cycle (**Figure 3B and 3C**). Light stimulation of GABA^{NTS}→ARC terminals induced a strong acute inhibition of food intake that lasted 60 min from food presentation, as compared to the same mice without light stimulation (**Figure 3D and 3E**).

The DVC has been proposed to be a key region modulating food intake reduction associated with aversive states (D'Agostino & Luckman, 2022). To assess whether GABA^{NTS}→ARC activation produces aversion or negative valence (Berridge, 2004; Betley et al., 2015), we evaluated the existence of passive avoidance behavior using an adapted real-time place preference (RTPP) task (D'Agostino et al., 2016; Kim et al., 2013; Stamatakis & Stuber, 2012). Specifically, in a two-sided open arena, light stimulus was coupled to one of the sides (**Figure 3F**). GABA^{NTS}→ARC stimulation or lack of stimulation did not produce a place preference (**Figure 3G**) and mice travelled a similar distance in both sides of the arena (**Figure 3H**). These findings indicate that GABA^{NTS}→ARC stimulation does not produce negative valence or aversion.

In addition to influencing homeostatic feeding, modulation of AgRP/NPY cells has also been reported to elicit anxiety-like behaviors influencing exploration and foraging which impacts food consumption (Dietrich et al., 2015; Heinz et al., 2021; Li et al., 2019). To test whether the activation of the GABA^{NTS}→ARC circuit produced anxiety-related behavior, mice were assessed in an open-field arena (OFA) and an elevated zero-maze task (EZM) (**Figure S2A and S2D**). GABA^{NTS}→ARC stimulation did not alter the time mice spent in the center of the OFA (**Figure S2B**). Likewise, mice displayed similar ambulatory patterns and travelled comparable distance during the OFA test with and without GABA^{NTS}→ARC stimulation (**Figure S2C**). Consistent with the OFA data, GABA^{NTS}→ARC stimulation did not alter either the time (**Figure S2E**) or distance travelled in the exposed zones of the EZM (**Figure S2F**).

These results provide evidence that stimulation of the GABA^{NTS}→ARC circuit impacts feeding without altering other behavioral states such as anxiety-like behavior.

We postulated that since our model involved fast neurotransmission rather than long term release of neuropeptides, the reduction in food intake that we observed could begin by reducing the interaction with the nutritional cue at first instance. To investigate this, we designed a task where mice would first be allowed to explore an empty arena and then three items would be presented at the same time, an inedible object, a novel palatable food item and a known nutritional food item (**Figure 3I**). The number of interactions with each item was measured with and without GABA^{NTS}→ARC stimulation. GABA^{NTS}→ARC stimulation did not induce changes in the interaction with the novel object (**Figure 3J**), further suggesting that GABA^{NTS}→ARC does not induce anxiety-like behavior. The number of interactions with the novel palatable food item was increased under both non-stimulation and stimulation trials (**Figure S2F and S2G**). However, we found that under optical stimulation mice had less interactions with the known nutritional item (**Figure 3J and S2G**), suggesting that GABA^{NTS}→ARC activation reduces hunger. Taken together, these findings indicate that GABA^{NTS}→ARC stimulation decreases feeding and hunger without inducing aversion or anxiety.

GABA^{NTS}→ARC neuron activation promotes satiety

We next used a two-virus intersectional approach (Fenno et al., 2014, 2017) to provide a more detailed characterization of GABA^{NTS}→ARC activation in energy homeostasis. *Vgat^{Cre}* mice were bilaterally injected with AAVs expressing Flipase recombinase (FlpO) (AAV-DIO-FlpO) under the control of Cre into the NTS of *Vgat^{Cre}* mice, allowing us to express a second recombinase only in GABA^{NTS} cells. After surgery recovery, a retrograde AAV encoding for a FlpO dependent hM3Dq-mCherry (rgAAV-fDIO-hM3Dq-mCherry) was bilaterally injected into the ARC to retrogradely deliver hM3Dq in a FlpO-dependent manner to GABA^{NTS} cells. Therefore, hM3Dq was expressed only in GABA^{NTS} cells projecting to the ARC in *Vgat^{Cre}* mice (**Figure 4A**).

Corroborating the optogenetic data presented above, the selective chemogenetic stimulation of the GABA^{NTS}→ARC circuit significantly reduced acute food intake (**Figure 4B** and **4C**) in ad libitum fed mice. GABA^{NTS}→ARC circuit activation did not alter overall locomotor activity

(**Figure 4D** and **4E**), respiratory quotient (**Figure 4F** and **4G**) or heat production (**Figure 4H** and **4I**). GABA^{NTS}→ARC neuron activation also reduced food intake in refed mice after overnight fasting (**Figure 4J**). Fasting is associated with a rise in systemic levels of ghrelin (Cummings et al., 2001) which acts as a pre-prandial effector stimulating AgRP/NPY neurons to initiate a feeding response (H. Y. Chen et al., 2004; Luquet et al., 2007). To examine whether GABA^{NTS}→ARC neuron activation is sufficient to dampen a hunger cue, GABA^{NTS}:hM3Dq-expressing mice were pre-treated with CNO prior to ghrelin. Activation of the GABA^{NTS}→ARC neurons with CNO prevented the feeding induced by an orexigenic dose of ghrelin (**Figure 4L and 4M)**. We next performed an analysis of the microstructure of the feeding event during the anorectic episode produced by CNO (Clifton, 2000; Richard et al., 2011; Zorrilla et al., 2005). GABA^{NTS}→ARC neuron activation reduced meal size (**Figure 4N**) and significantly reduced the number of meal events in the earliest interval compared to saline treatment (**Figure 4O** and **4P**). Taken together, these findings indicate that GABA^{NTS}→ARC neuron activation is sufficient to blunt fasting and ghrelin-induced hunger and significantly reduces food intake by promoting satiety.

Discussion

Here we identify a critical new brain circuit modulating appetite and body weight. We focused on the NTS because it is a brain region positioned to receive and integrate energy-related information from the periphery and relay it within the CNS to promote energy homeostasis. However, the NTS is neurochemically heterogeneous and key neurons within it performing this function have not been fully defined. Using multi-methodological approach, here we identify GABA^{NTS} neurons as sufficient to control feeding behavior and body weight in mice.

Recent efforts to decode the function of specific chemically defined neurons within the NTS have revealed that distinct subpopulations of glutamatergic cells play a role in energy homeostasis (Dowsett et al., 2021). However, NTS inhibitory GABA-releasing neurons have not been studied in detail and this is necessary to clarify the role of both excitatory and inhibitory NTS signals in the regulation of energy balance (Cheng et al., 2022). Here we provide a detailed characterization of the effect of GABA^{NTS} in the regulation of energy homeostasis and body weight. A recent report provided evidence that obesity medication liraglutide engages GABA^{NTS} neurons to reduce food intake in rats, providing a rationale that

activating GABA^{NTS} cells may have translational relevance for the treatment of human obesity (Fortin et al., 2020).

The NTS is involved in satiety and satiation, and refeeding induces a strong neuronal activation in this region (D'Agostino et al., 2016; Wu et al., 2014). We discovered that refeeding significantly activates a subset of GABA^{NTS} cells. Further, we found that activation of GABA^{NTS} neurons with chemogenetics was anorectic, and controlled food intake and body weight. Consistently, when we inhibited these neurons, we observed a potent induction of feeding in satiated mice, suggesting a crucial role in the induction of early eating. However, when the inhibition occurred in ad libitum mice entering the dark cycle, we didn't observe an increased food intake. This could be explained by two reasons. First, despite of mice being kept in ad libitum conditions, they are not satiated at the onset of the dark cycle, meaning GABA^{NTS} neuros are likely to not be active at this time, therefore an inhibition would not meaningful. Second, during the active dark cycle there are multiple feeding cues not only vagal sensory afferents but afferent from the sensory system that would modulate feeding and could counteract GABA^{NTS} lack of inhibition in second order neurons. Our data illustrates that GABA^{NTS} neurons project widely within the brain, with particularly dense innervation of the hypothalamus. Several studies indicate that there is a coordination between the NTS and the hypothalamus to orchestrate the meal event (Aklan et al., 2020; Blevins et al., 2004; D'Agostino et al., 2018; Liu et al., 2017; Tsang et al., 2020). However, whether the ARC receives inhibitory control from the NTS is not known and was examined here.

Given that GABA is an inhibitory neurotransmitter, we hypothesized that GABA^{NTS} neurons inhibit appetite stimulating neurons. We focused on AgRP/NPY^{ARC} neurons because of the dense GABA^{NTS} innervation that we found and the potent orexigenic properties of AgRP/NPY (Aponte et al., 2011; Krashes et al., 2011; Luquet et al., 2005). In addition, AgRP/NPY neurons display a multiple timescale activation (Mandelblat-Cerf et al., 2015) that could explain the lack of feeding effect during the chemogenetic inhibition of GABA^{NTS}. We demonstrated that GABA^{NTS} terminals in the ARC release GABA and that this is synchronized with suppression of the action potential propagation postsynaptic AgRP/NPY^{ARC} cells. The timescale of $GABA_AR$ openings after optical stimulation in a membrane patch placed over the GABA^{NTS} terminal suggests the release of GABA from this terminal rather than from another inhibitory neurons. The number of AgRP/NPY neurons responding is in line with the 20% ARC responders to NTS innervation published previously (Aklan et al., 2020). However, despite the relatively small number of AgRP/NPY^{ARC} neurons inhibited by GABA^{NTS} terminals,

it was sufficient to significantly reduce feeding in freely behaving mice. AgRP/NPY cells are poised to orchestrate the integration of homeostatic, reward and sensory cues as well as learning and conditioned behaviors (Aponte et al., 2011; Berrios et al., 2021; Deem et al., 2022; Dietrich et al., 2012, 2015; Garau et al., 2020; Han et al., 2021; Jikomes et al., 2016; Krashes et al., 2011, 2014; Wang et al., 2021). A detailed analysis of feeding behavior revealed that activation of the $GABA^{NTS}$→ARC pathway specifically reduces hunger and promotes satiety and does not induce negative valence, aversion or anxiety.

Obesity is an international health concern that is primarily the consequence of over-eating. Defining the mechanisms governing hunger and food intake is therefore of paramount importance. Here we identify a new player that controls appetite and body weight, $GABA^{NTS}$. Specifically, we show that NTS GABA-releasing neurons are active during satiety and reduce food intake and body weight without causing aversion or anxiety. We demonstrate that $GABA^{NTS}$ cells directly activate $GABA_AR$s on the surface of AgRP/NPY cells which inhibits neuron activity. These studies reveal for the first time the effect of $GABA^{NTS}$ neurons on feeding and body weight, and identify a fast inhibitory circuit between the NTS and the ARC in the control of food intake. These results thereby provide significant insight into the brain circuits governing appetite and body weight, findings of relevance to the global obesity crisis.

Methods

RNA-Seq

Single nucleus RNA-sequencing data from the mouse hindbrain in the fed and fasted state was taken from (Dowsett et al., 2021). Neuronal nuclei expressing at least 1 UMI count for *Slc32a1* were identified as GABAergic neurons, subsetted and reclustered using Seurat package version 4.3 (Hao et al., 2021). Marker genes for each cluster were calculated using Wilcoxon's rank-sum test. Each cluster was named with 2 marker genes that were expressed in >60% of the cluster, <30% of the rest of the data and had an average log fold change >0.5. If no genes fit these criteria, then the two genes with the lowest p-values were used. Differential gene expression analysis between ad libitum fed and overnight fasted cells was performed using the Wilcoxon's rank sum test. Feature plots were drawn using the Seurat package and ggplot2.

Animals

Vgat-ires-Cre (Vong et al., 2011) (Slc32a1tm2(cre)Lowl; #016962), *NPY-hrGFP* (van den Pol et al., 2009)(van den Pol et al., 2009)(van den Pol et al., 2009)(van den Pol et al., 2009) (B6.FVB-Tg(Npy-hrGFP)1Lowl/J; #006417), POMC-dsRed (Hentges et al., 2009) (Tg(Pomc-DsRed)18Low) and *Rosa26tdTomato-LoxP* (Madisen et al., 2009) (B6.Cg-Gt(ROSA)26Sortm9(CAG-tdTomato)Hze/J, #007909) mice were obtained from The Jackson Laboratory (Bar Harbor, USA) and bred in a C57Bl/6J background. Mice were fed with standard laboratory chow (Standard CRM (P) 801722, Special diets, UK) and provided with water ad libitum, unless otherwise stated. Mice were kept in a 12-hours light:dark cycle (7am-7pm) in environmental controlled conditions (20-22°C and 40-60% RH). All experimental procedures were performed in accordance with the UK Animal (Scientific Procedures) Act 1986.

Viral vectors

Cre-dependent viral vectors were purchased from Addgene, AAV8-hSyn-DIO-hM3D(Gq)-mCherry ($1.83x10^{12}$ gc/ml) was a gift from Bryan Roth (Addgene plasmid # 44361) (Krashes et al., 2011), AAVrg-hSyn-fDIO-hM3D(Gq)-mCherry-WPREpA ($1.8x10^{12}$ gc/ml) was a gift from Ulrik Gether (Addgene plasmid # 154868); AAV8-hSyn-DIO-mCherry ($3.6x10^{12}$ gc/ml) was a gift from Bryan Roth (Addgene plasmid # 50459); AAV8-pEF1a-DIO-FLPo-WPRE-

hGHpA ($2x10^{12}$ gc/ml) was a gift from Li Zhang (Addgene plasmid # 87306) (Zingg et al., 2017). AAV2-EF1a-DIO-ChR2(E123T/T159C)-mCherry and AAV2-EF1a-DIO-ChR2(E123T/T159C)-YFP ($7.3x10^{12}$ vp/ml) were a gift from Karl Deisseroth and were obtained from University of North Carolina Vector Core (Chapel Hil, NC, USA). All viral particles were delivered into nuclei-specific regions through stereotaxic injections.

Stereotaxic surgeries

For viral delivering in the NTS, stereotaxic surgery was adapted from previous studies (D'Agostino et al., 2016). Briefly, 12-20 weeks old mice were anaesthetized with isoflurane, back region of the neck shaved and placed in a stereotaxic instrument (David Kopf instruments, CA, USA) with a face mask (World Precision Instruments, FL, USA). Head was inclined ~70 degrees forward and a longitudinal incision was made in the skin at the level of the C1; neck muscles were retracted to expose the atlanto-occipital membrane. This was carefully dissected allowing access to the dorsal brainstem and visualization of the obex. Using a pulled glass capillary (40µ tip diameter) (G1, Narishige, UK) and a pneumatic microinjector (IM-11-2, Narishige, UK) 200-300 nl of viral preparation was bilaterally injected into the NTS (obex: AP:0.25 mm AP, L:± 0.25 mm and DV:-0.25mm) at a flow of 50nl/min. Capillary was left in the injection place for 5 min to allow diffusion and it was removed slowly to avoid dispersion to neighbor brainstem regions. Viral delivery into the ARC was performed as previously described (Wagner et al., 2022) at coordinates bregma: AP:1.58 mm AP, L:±0.2mm and DV:5.90 mm. For optical fiber cannula placement, mice were allowed 4 weeks recovery form the NTS surgery and a 200 µm core diameter, 0.39NA (CFMLC, Thorlabs, UK) optical fiber implants were placed in the third ventricle above the ARC. Mice were allowed 3 weeks before any study to allow surgery recovery and maximal viral expression. Post hoc analysis of injection site, viral expression and canula placement were used as exclusion criteria for data analysis.

In vivo photo-stimulation protocol

Optical fiber implants were attached to optogenetics patch cables (M83L1, Thorlabs, UK) connected to a rotary joint (Doric lenses) coupled to a 473-nm laser (Laserglow, Toronto, Canada) controlled via TTL-USB interface with Arduino board. For feeding experiments, the

425 stimulation protocol was 1 s followed by 4 s break with 10ms light pulses with a frequency of
426 30Hz. For behavioral experiments, the stimulation protocol was 1 s followed by 0.5 s break
427 with 10ms light pulses with a frequency of 30Hz. We used 15mW of laser power to achieve
428 an irradiance of 5-10mW/mm^2 (PM100D, Thorlabs) on the target area following
429 https://web.stanford.edu/group/dlab/cgi-bin/graph/chart.php, above ChR2 threshold
430 activation (Lin et al., 2009).

431

432 **Food intake and body weight studies**

433 For food intake, body weight and metabolic parameters measurements, mice were single
434 housed and habituated in indirect calorimetry system cages for one week (Phenomaster, TSE
435 Systems, Germany). For acute ad libitum studies, access to food was removed in fed mice
436 2h before entering the dark cycle and CNO 1 mg/kg was i.p. administered 30 min before the
437 dark cycle onset when food was provided. For re-feeding studies, 12 hours dark cycle-food
438 deprived mice were i.p. injected with CNO at the beginning of the light cycle and 30 min after
439 food was provided. For subchronic studies, mice were i.p. injected twice a day (am and pm)
440 for 5 days with CNO following 5 days with saline.

441

442 **Behavioral tests**

443 For valence studies, mice were assessed in an adapted real-time place preference task
444 consisting in an open field arena with two connected identical chambers (30x25cm)
445 (D'Agostino et al., 2016; Kim et al., 2013; Stamatakis & Stuber, 2012), one of them paired
446 with optogenetic stimulation where mice were allowed free movement for 20 min. For anxiety
447 tests, mice were placed in an open arena (50x50cm) with virtual delimited central and
448 peripheral regions and allowed free movement for 10 minutes with and without stimulation in
449 different days. For anxiety and fear assessment, mice were placed in an elevated zero maze
450 (diameter 50cm, elevation 70 cm) with 2 hidden and 2 exposed zones and allowed free
451 movement between zones for 10 min. Tests were performed for each animal with and without
452 stimulation in different days. Time and locomotor parameters for each task and zone were
453 recorded using Any-Maze software (Stoelting, IL, USA).

454

Immunohistochemistry and imaging

All mice were injected with a terminal dose of anesthesia and transcardially perfused with phosphate-buffered saline (PBS) followed by 10% neutral buffered formalin. Brains were dissected, post-fixed 12 hours in formalin at 4°C, cryoprotected 48 hours with 30% sucrose 4°C and coronally sectioned in 5 series at 25 µm using a freezing microtome (8000, Bright Instruments, UK). Sections were kept in protective anti-freeze solution at 4°C until they were processed for immunohistochemistry as previously described (Yavari et al., 2016). Briefly, NTS sections were washed with PBS-0.2% Tween20 30 min and then PBS (3x10 min), blocked with 1%BSA/5%DS/0.25%Triton X-100 1 hour at room temperature and incubated with primary antibody in blocking solution with anti-c-Fos (1:2500, 2250, CST, USA), anti- c-Fos (for chromogenic) (1:5000, ABE457,Merck, UK), anti-mCherry (1:2000, AB0040-200, Scigen, PT), anti-RFP (1:1000, 600-401-379, Rockland Immunochemicals, USA), anti-POMC (1:3000, H-029-30, Phoenix Pharmaceuticals, USA), anti-hrGFP (1:2000, 240141, Agilent, USA), anti-TH (1:2000, MAB318, Merck, Germany) 16 hours at room temperature. The next day, sections were washed with PBS-Tween and PBS and incubated 1 hour with appropriate secondary antibodies in blocking solution (1:500, AlexaFluor594, AlexaFluor488, Invitrogen, UK) at room temperature. For c-Fos expression quantification in fast vs refed study, chromogenic staining with DAB reagent was performed as previously described (D'Agostino et al., 2016).

Images were acquired using Axioskope2 microscope and Axiovision software (Zeiss, Germany). All images were converted to 8-bit, peudorecolored and cells counted using ImageJ (Fiji).

Electrophysiology

CRACM study

CRACM experiments were performed as previously described (González et al., 2016). Six *Vgat*^{Cre}:*Npy*^{hrGFP} mice and six *Vgat*^{Cre}:*Pomc*^{dsRed} mice bilaterally injected with AAV-ChR2-mCherry and AAV-ChR2-mCherry respectively into the NTS, aged between 5 and 7 months at the time of the electrophysiology experiments, were used. Expression of mCherry-ChR2 was targeted to NTS^{GABA} cells by stereotaxic injection of AAV as above. Coronal brain sections 180-µm thick were prepared from these mice at least 8 days after virus injections

and were placed in a bath solution consisting of (in mM) 125 NaCl, 2.5 KCl, 1.2 NaH_2PO_4, 21 $NaHCO_3$, 1 glucose, 2 $MgCl_2$, 2 $CaCl_2$. GFP-expressing cells in the ARC were identified using an upright microscope (Scientifica S-Scope-II) equipped with the appropriate fluorescence filters. Whole-cell recordings from these cells were obtained with glass pipettes (World Precision Instruments 1B150F-4) filled with a solution containing (in mM) 120 K-gluconate, 10 HEPES, 10 KCl, 1 EGTA, 2 MgCl2, 4K2ATP, and 1 Na2ATP, tip resistance 3-7 MOhm. Data was acquired using Axon Instruments hardware (MultiClamp 700B, Digidata 1550). To test for GABA inputs to AgRP/NPY^{ARC} cells, the membrane potential in these cells was clamped at increasing levels of voltage (from -100 to -10 mV in 10-mV increments), while ChR2-expressing terminals were stimulated by a single light pulse (CoolLED pE-4000) to induce post-synaptic currents. Liquid junction potential, estimated to be 10 mV, was subtracted from the measurements. Chloride equilibrium potential was calculated to be -60.3 mV.

Sniffer-patch recordings

Transverse hypothalamic slices from *Vgat*^{Cre}:*Npy*^{hrGFP} mice bilaterally injected AAV-DIO-ChR2-mCherry were cut at 200-250 using a Leica VT1200S vibratome. Slices were incubated for one hour in a solution containing (in mM): 124 NaCl, 3 KCl, 1 $CaCl_2$, 3 $MgCl_2$, 26 $NaHCO_3$, 1.25 NaH_2PO_4, 10 D-glucose, and bubbled with 95/5% O_2/CO_2, pH 7.4. After incubation, slices were transferred to a recording chamber continuously superfused with an external solution. The external solution composition differed from incubation solution in containing 2 mM $CaCl_2$ and 2 mM $MgCl_2$.

In all experiments the intracellular pipette solution for voltage-clamp recordings contained (mM): 117.5 Cs-gluconate, 17.5 CsCl, 10 KOH-HEPES, 10 BAPTA, 8 NaCl, 5 QX-314, 2 Mg-ATP, 0.3 GTP; for current-clamp recordings: 126 K-gluconate, 4 NaCl, 5 HEPES, 15 glucose, 1 $MgSO_4 \cdot 7H_2O$, 2 BAPTA, 3 Mg-ATP (pH 7.2, 295-310 mOsm in both cases); pipette resistance was 7-9 MOhm; recordings were performed at 33-35ºC using Multiclamp-700B amplifier with -60 or -70 mV holding current (for voltage-clamp recordings); signals were pre-filtered and digitized at 10 kHz. In experiments where transmembrane currents were recorded in outside-out patches only (sniffer-patch recordings), the $GABA_A$ receptors response was isolated with a ligands cocktail containing 50 µM APV, 20 µM NBQX, 50 nM CGP-55845, 200 µM S-MCPG, 10 µM MDL-72222, and 1 µM strychnine.

Statistics and data analysis

Statistical analyses were performed using GraphPad Prism 9 software and are described in the figure legend where 2-tail paired and unpaired Student t-test were used when comparing 2 groups and RM/two-way ANOVA test with Bonferroni post-hoc correction when comparing 4 groups. RNA-Seq data were analyzed as described above. No statistical method was used to predefine sample size, randomization and blinding was performed for histological quantifications. Statistical significance was accepted when the $p \leq 0.05$. Raw data was stored in Excel and figures assembled with CorelVector and Affinity Designer software.

Author Contributions

The project was conceived by PBM and LKH. PBM designed and performed experiments and analyzed data with assistance from YM; GKCD and GSHY performed and analyzed the RNA-Seq data. SS and AG designed and performed electrophysiological recordings. The manuscript was drafted by PBM with input from all other authors.

Acknowledgements

We gratefully acknowledge Dr F. Naneix for advice on optogenetics and editorial advice, and staff within the University of Aberdeen Medical Research Facility and the Microscopy Facility for their technical assistance. This work was supported by the ERC (MSCA-IF-NeuroEE-660219) to PBM, Wellcome Trust Institutional Strategic Support Fund (204815/Z/16/Z) to PBM and LKH, and the Biotechnology and Biological Sciences Research Council (BB/V010557/1) to JAG and (BB/V016849/1) to LKH and SS. GKCD is funded by a BBSRC CASE 4-year PhD studentship, co-funded by Novo Nordisk. GSHY is funded by the UK Medical Research Council (MC_UU_00014/1).

Conflict of interest

The authors declare no competing financial interests.

546 **Figure 1**

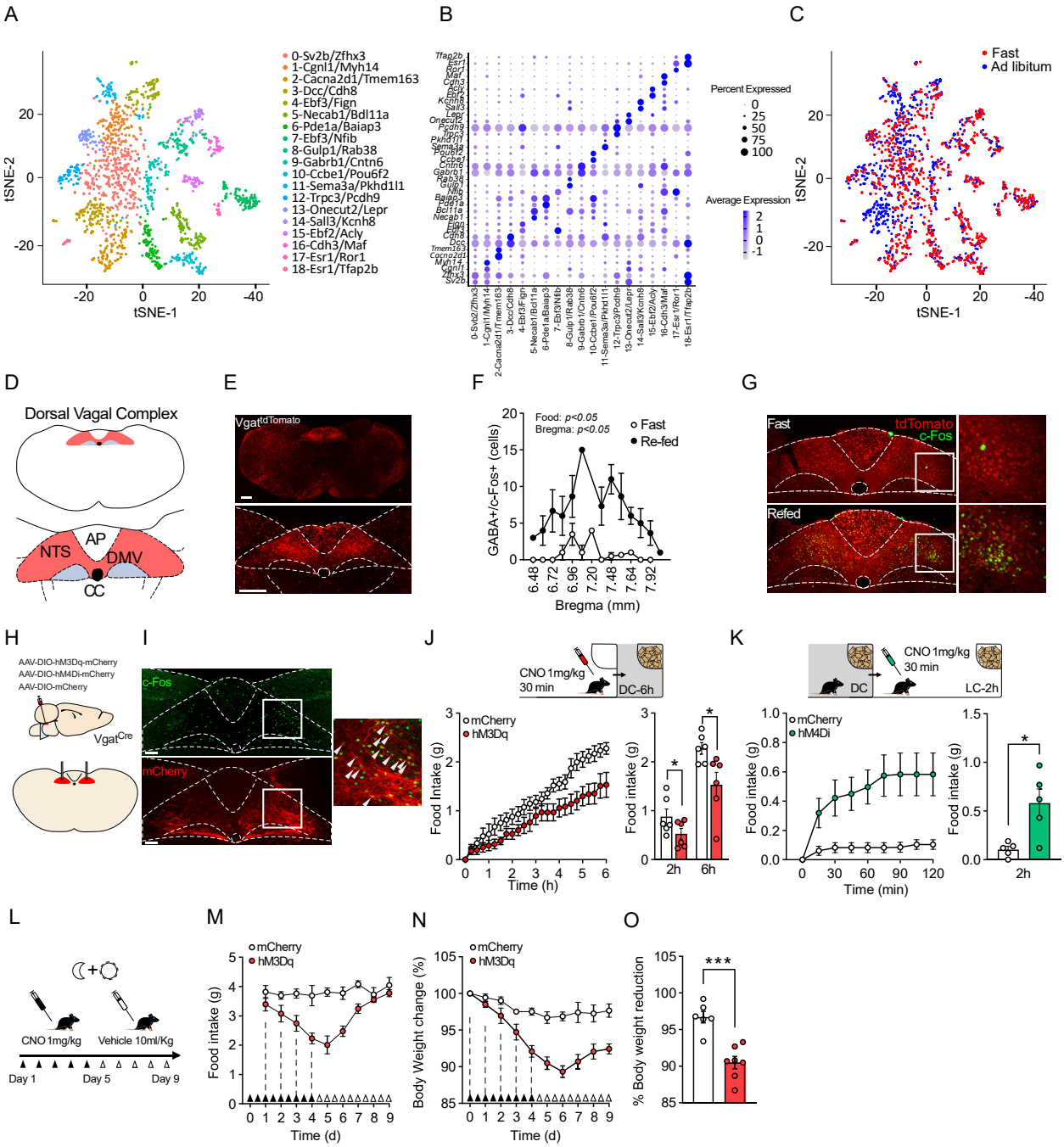

547

548

Figure 2

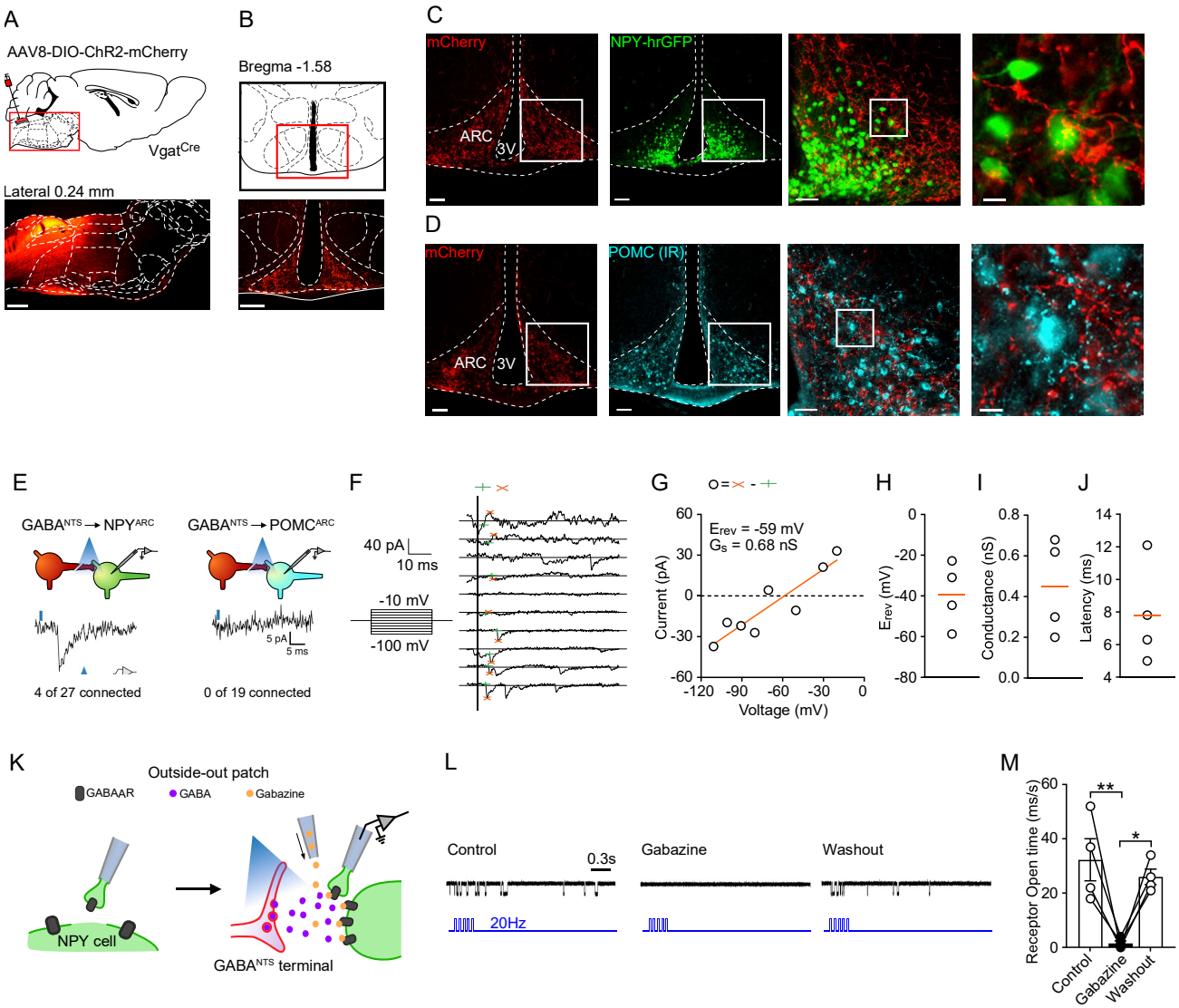

552 **Figure 3**

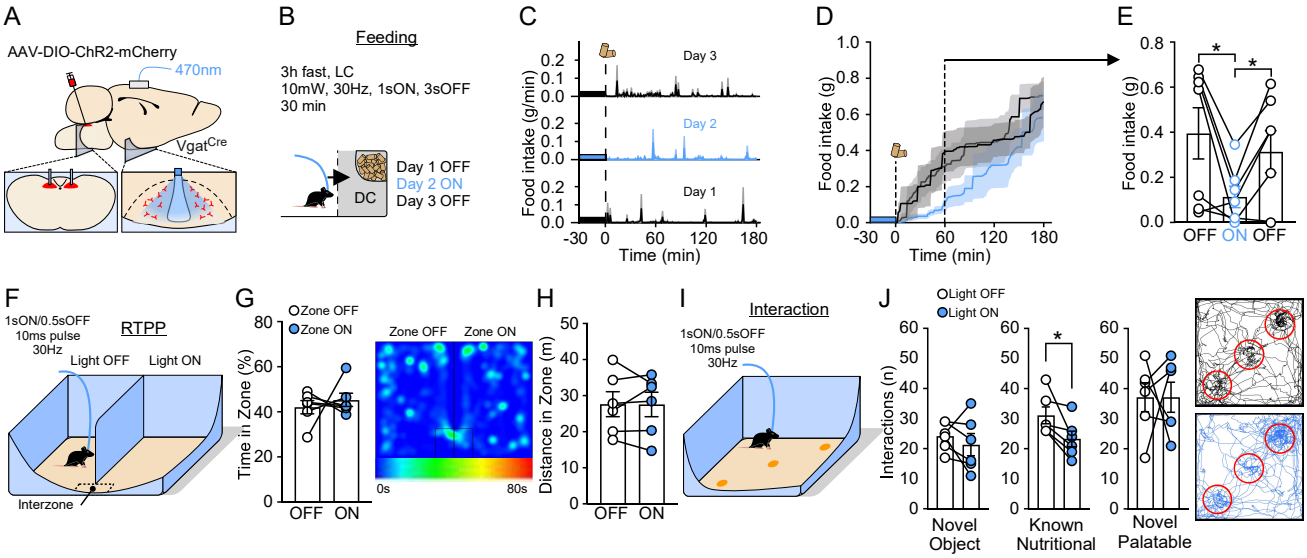

553

554

Figure 4

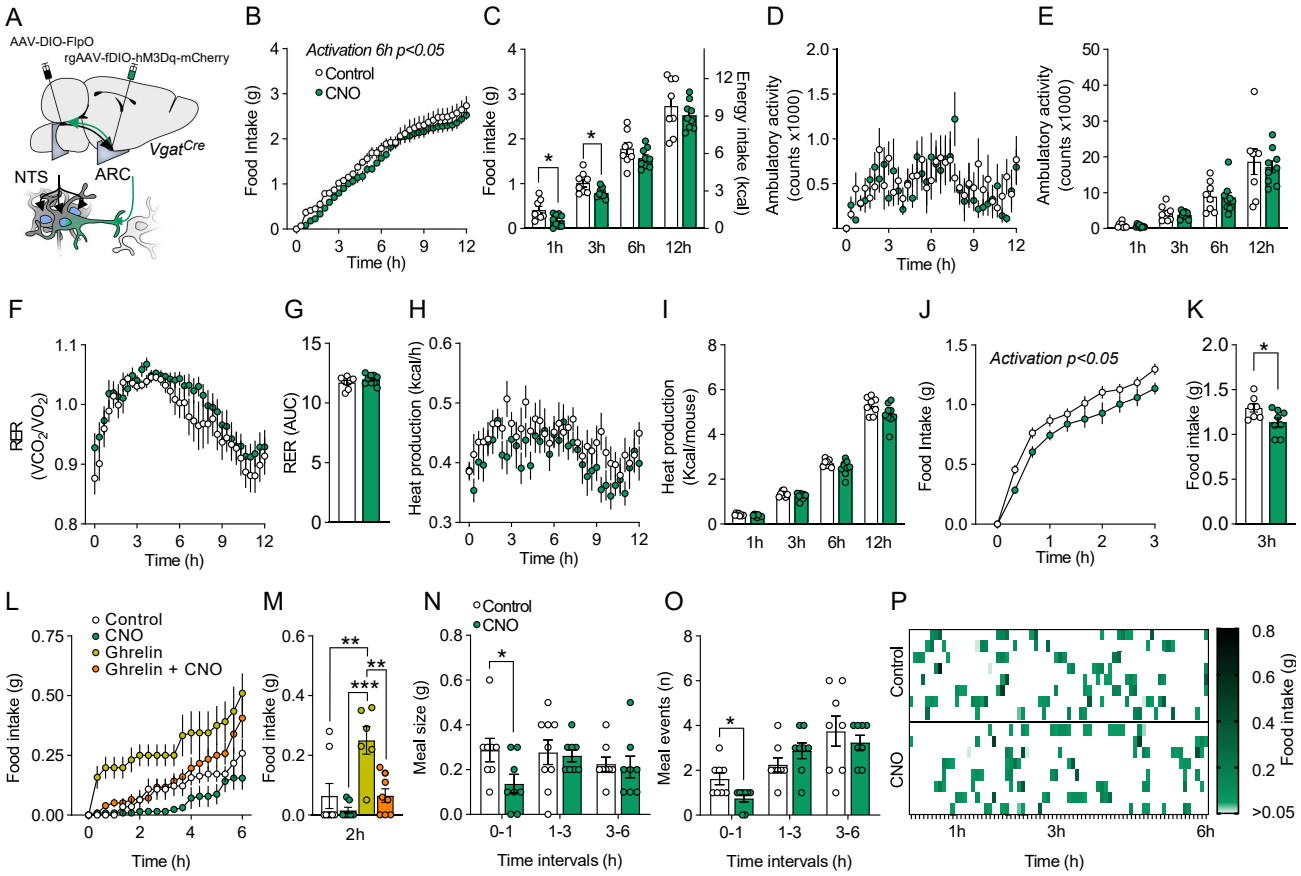

Supplementary Figure 1

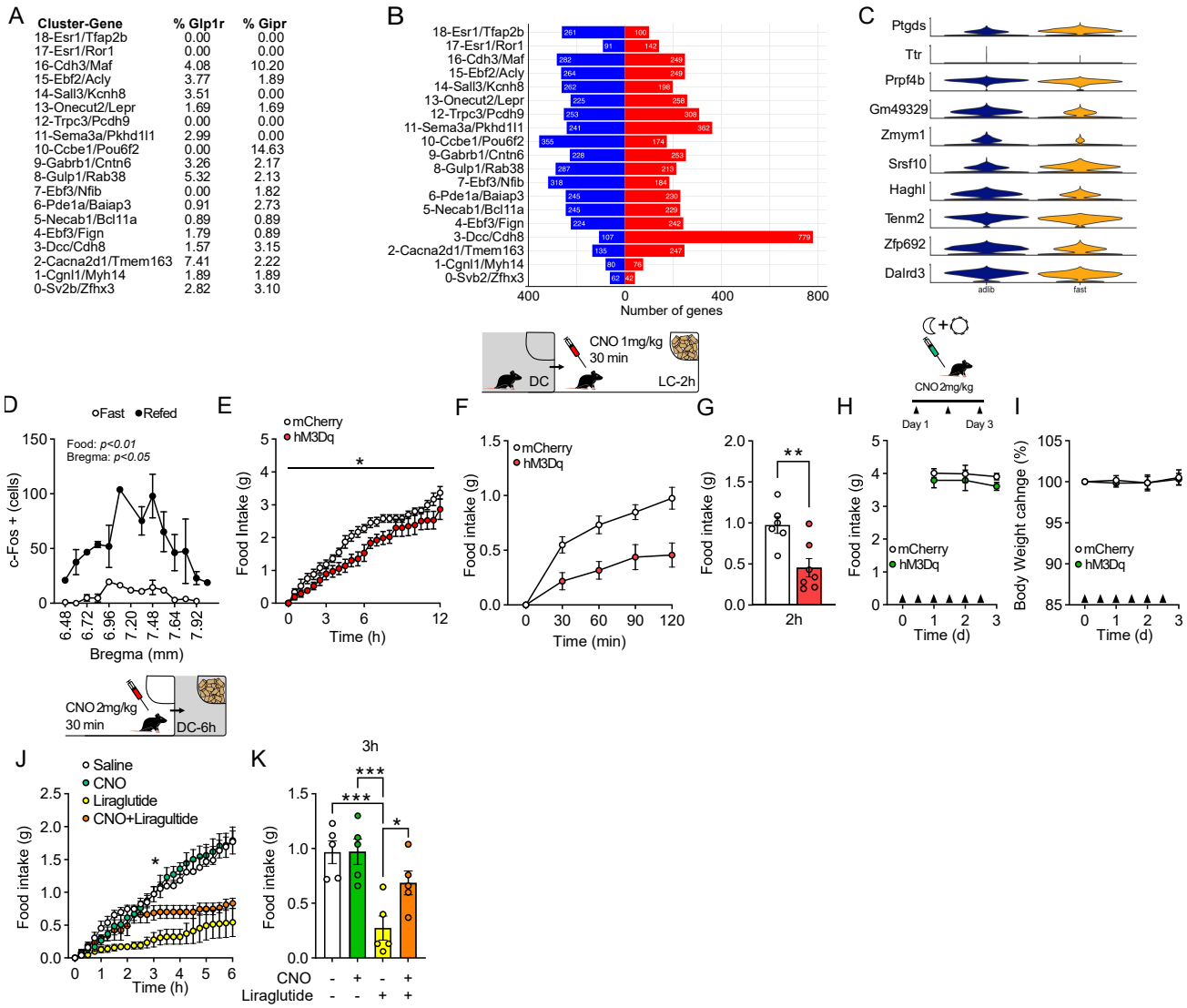

Cluster-Gene	% Glp1r	% Gipr
18-Esr1/Tfap2b	0.00	0.00
17-Esr1/Ror1	0.00	0.00
16-Cdh3/Maf	4.08	10.20
15-Ebf2/Acly	3.77	1.89
14-Sall3/Kcnh8	3.51	0.00
13-Onecut2/Lepr	1.69	1.69
12-Trpc3/Pcdh9	0.00	0.00
11-Sema3a/Pkhd1l1	2.99	0.00
10-Ccbe1/Pou6f2	0.00	14.63
9-Gabrb1/Cntn6	3.26	2.17
8-Gulp1/Rab38	5.32	2.13
7-Ebf3/Nfib	0.00	1.82
6-Pde1a/Baiap3	0.91	2.73
5-Necab1/Bcl11a	0.89	0.89
4-Ebf3/Fign	1.79	0.89
3-Dcc/Cdh8	1.57	3.15
2-Cacna2d1/Tmem163	7.41	2.22
1-Cgnl1/Myh14	1.89	1.89
0-Sv2b/Zfhx3	2.82	3.10

559

560

Supplementary Figure 2

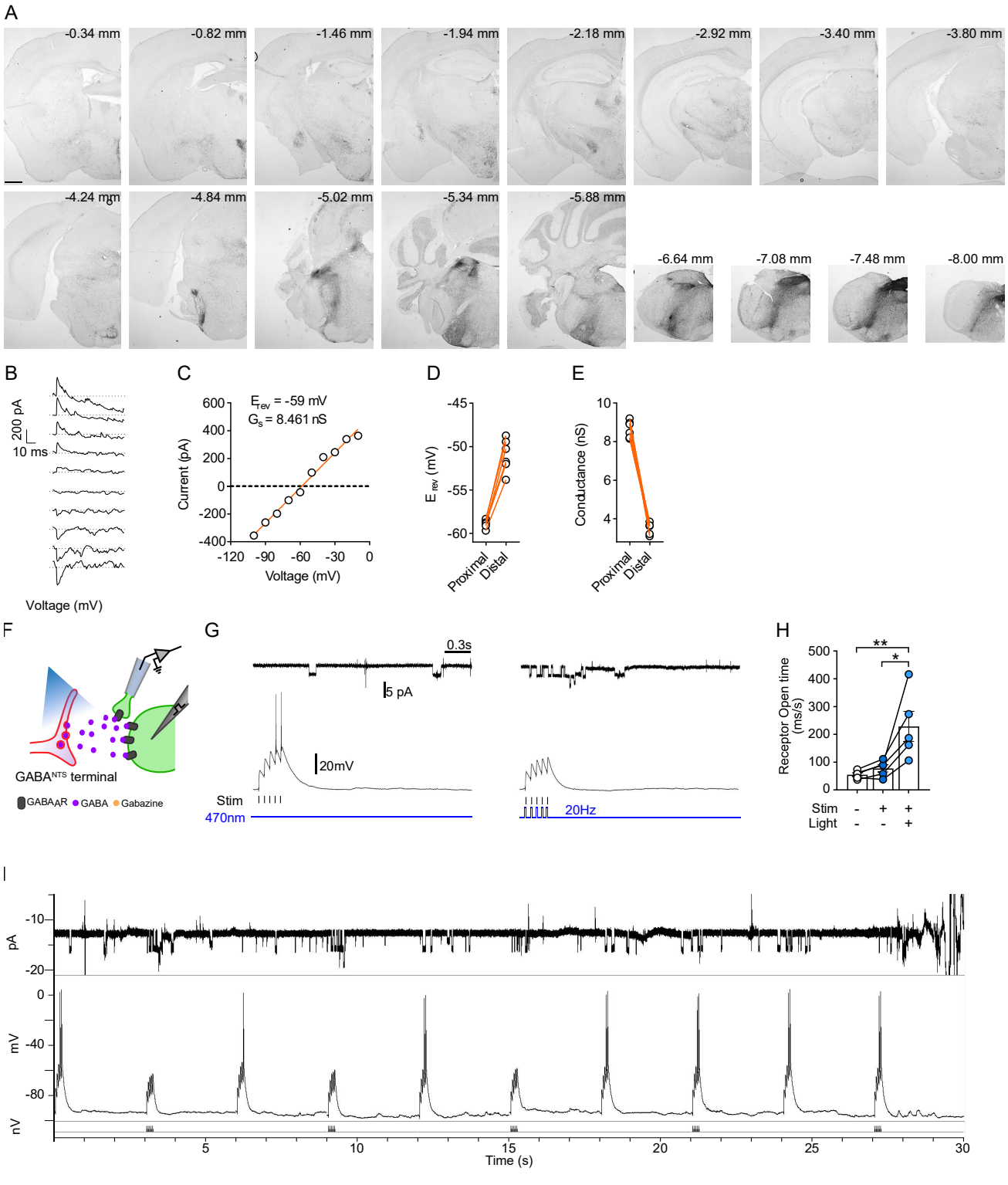

562

563

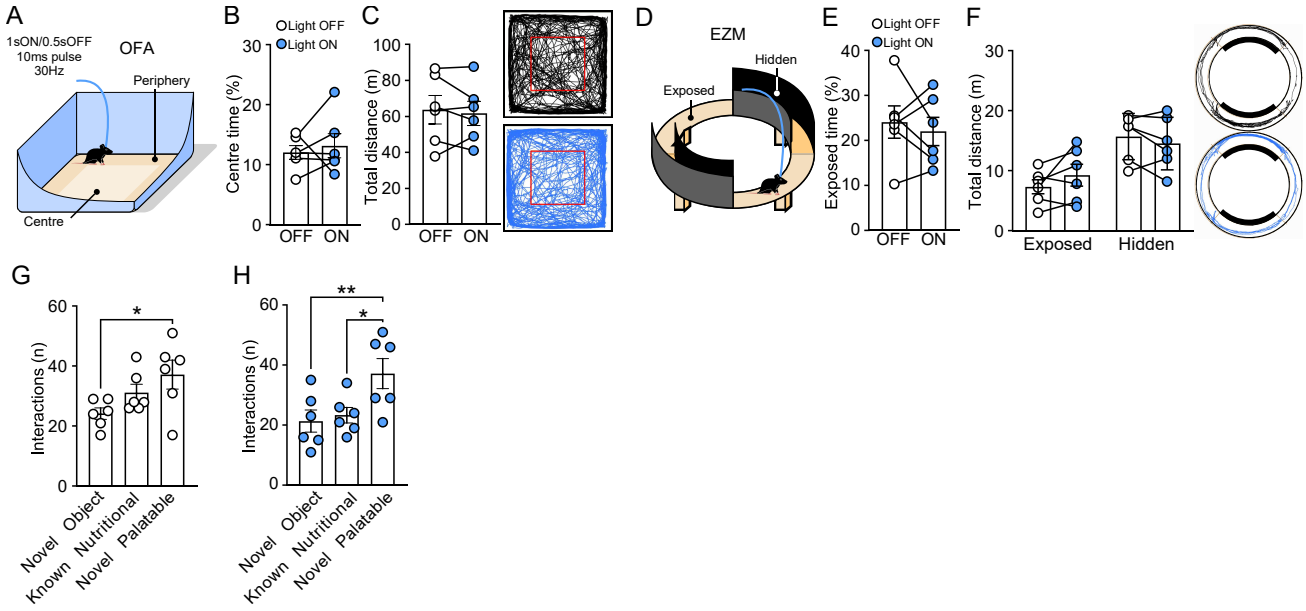

564

565

Figures Legends

Figure 1. GABA^{NTS} activation reduces food intake and body weight. (A) tSNE plot of *Slc32a1*$^{+}$ neurons in the DVC colored by cluster, (B)Dot plot showing scaled expression of marker genes for each of the 19 *Slc32a1*$^{+}$ clusters (C) tSNE plot of the *Slc32a1*$^{+}$ nuclei colored by nutritional status (D) Schematic of the DVC (top) with zoom-in diagram showing AP, NTS and DMC (bottom). (E) Representative photomicrograph of GABAergic cell distribution in the medial brainstem (top) and in the DVC (bottom) using *Vgat*^{tdTom} mice. (F) Quantification GABAergic cells expressing c-Fos following 16h fasting and fasting+2h refeeding (n=3, Bregma level: two-way ANOVA $F_{(13,34)}$=2.63; p=0.012; Nutritional state: two-way ANOVA $F_{(1,4)}$=8.69; p=0.042. (E) Representative micrograph of *Vgat*^{tdTom} cells (red) expressing c-Fos (green) in mice fasted 16h (top) and re-fed for 2h (bottom). (H) Schematic of AAV-DIO-hM3Dq/hM4Di/mCherry infused into NTS of *Vgat*^{Cre} mice. (I) Representative photomicrograph of c-Fos (green) expression in hM3Dq-mCherry (red)-expressing cells in the NTS of VgatCre mice treated with CNO (1 mg/kg, i.p) and (J) 6h cumulative and (J) 2h and 6h total food intake (n=6, Unpaired t test $t_{(11)}$=2.663, p=0.0238) of GABA^{NTS}:hM3Dq CNO injected mice compared to mCherry. (K) 2h cumulative and (J) 2h total food intake (n=5, Unpaired t test $t_{(8)}$=3.205, p=0.0125) GABA^{NTS}:hM4Di CNO injected mice compared to mCherry. (L) 10-day treatment protocol schematic. Daily CNO treatment significantly reduced (M) food intake (RM two-way ANOVA $F_{(1,11)}$=20.57; P=0.0008), (N) body weight (n=6/7, RM two-way ANOVA ($F_{(1,11)}$=21.96; p=0.0007) and (O) body weight change GABA$^{NTS:hM3Dq}$ mice compared to control GABA^{NTS}:mCherry mice (n=6/7, Unpaired t test $t_{(11)}$=5.252, p=0.0003). C-D n=4/group, H-K n=6; M-O n=6 mCherry and n=7 hM3Dq. Data represented as mean±S.E.M. *: p<0.05; **: p<0.01; ***: p<0.001. AP: Area Postrema; CC: Centre canal; DMV: Doral motor nucleus of the vagus nerve; NTS: Nucleus of the solitary tract.

Figure 2. GABA^{NTS} projections to the ARC release GABA into AgRP/NPY neurons. (A) Illustration depicting details for NTS injection of AAV-DIO-ChR2-mCherry (top) and representative photomicrograph (scale 1mm) of injection (bottom) in *Vgat*^{Cre} mice and (B) ChR2-mcherry containing fibers in the ARC (scale 200um). (B) Representative photomicrographs (scale 100um) and magnification (scale 50 and 10um) ChR2-mCherry fibers in the ARC close to NPY^{hrGFP}-expressing cells and (D) POMC-expressing cells and in *Vgat*^{Cre} mice bilaterally injected AAV-DIO-ChR2-mCherry. (E-J) *Vgat*^{Cre}:*Npy*^{hrGFP} mice CRACM study. (E) Representative membrane potential response of NPYGFP and POMCDsRed cells after light stimulation of mCherry containing terminals. (F) Representative membrane current in Npy^{hrGFP} cell recorded during a voltage-clamp experiment from -100mV to -10mV in 10-mV steps. (Vertical line: light pulse; green cross: base line; red cross: peak value). (G) Representative light-induced post-synaptic current during voltage clamp experiment showing peak conductance, G_s, and reversal potential, E_{rev}. (H) Individual values and median of (H) E_{rev}, (I) Conductance, G_s and (I) latency of all responsive cells. (K) Diagram of outside-out patch technique in *Vgat*^{Cre}:*Npy*^{hrGFP} mice bilaterally injected AAV-DIO-ChR2-mCherry. (L) Representative channel opening recordings of control (left) gabazine (middle) and washout (right) recordings. (M) Quantification of receptor opening time (n=4, RM two-way ANOVA $F_{(2,6)}$=16.14; p=0.0039, Bonferroni adjusted p=0.0051 Control vs Gabazine and p=0.0156 Gabazine vs Washout. Data in M are expressed as mean±S.E.M. E-J: 4/27 cells NPYhrGFP and 0/19 cells POMCdsRed; K-M: n=4-5 patches. *: p<0.05; **: p<0.01.

Figure 3. Activation of GABA^{NTS}→ARC projections reduces food intake without inducing aversion. (A) Schematic of viral infection and optic fiber placement for in vivo stimulation of GABA^{NTS}→ARC. (B) Protocol of stimulation. (C) Representative 1min resolution time plot of 3h food intake measurement. GABA^{NTS}→ARC stimulation significantly reduces (D) cumulative 3h food intake and (E) 60min intake (n=7, day 1 (OFF) vs day 2 (ON) paired Student t-test $t_{(6)}$=3.035, p=0.0229; day 2 (ON) vs day 3 (OFF) paired Student t-test $t_{(6)}$=3.283, p=0.0168). (F) Diagram illustrating RTPP task. GABA^{NTS}→ARC does not alter (G) time spent (representative heat map of time) or (H) distance travelled in stimulated and non-stimulated zones. (I) Diagram illustrating an object interaction task. (J) Interactions with novel, known nutritional or novel palatable objects and a representative path track around each object (red circle). GABA^{NTS}→ARC stimulation reduced interaction with known nutritional item (n=6, Student's t test $t_{(5)}$=3.043, p=0.0287). Data are expressed as individual values and as mean±S.E.M, n=6 mice. *: p<0.05; RTPP: real-time place preference.

Figure 4. Chemogenetic activation of GABA^{NTS}→ARC neurons induces satiety. (A) Diagram illustrating the two-virus intersectional strategy to express hM3Dq only in GABA^{NTS} neurons projecting to the ARC. Mice were treated with saline or CNO (1 mg/kg, i.p.). (B) CNO significantly reduced cumulative food intake over 6h (0-6h $F_{(1,15)}$=7.418, p=0.0157), (C) 1h (Unpaired t-test $t_{(15)}$=2.648, p=0.0183) and 3h (Unpaired t-test, $t_{(15)}$=2.568 P=0.0214) food intake compared to saline. (D) CNO did not alter 12h or (E) 1, 3, 6 or 12h quantification of ambulation; (F) 12h RER or (G) AUC quantification; (H) 12h or (I) 1, 3, 6 and 12h heat production per mouse compared to saline. (J-K) CNO significantly reduced 3h food intake following overnight fasting (J, 2-way ANOVA $F_{(1.13)}$=6.139, p=0.0277 and K, unpaired t-test $t_{(13)}$=2.320, p=0.0372). (L-M) CNO attenuated ghrelin hyperphagia over 2h (RM ANOVA $F_{(3,16)}$=11.12; p=0.0003, Bonferroni adjusted p=0.0042 control vs ghrelin, p=0.0003 CNO vs ghrelin and p=0.002 Ghrelin vs Ghrelin+CNO). (N) CNO reduced meal size (Unpaired t-test, $t_{(14)}$=2.256, p=0.0406) and (O-P) decreased meal number (Unpaired t-test, t(14)=2.824, p=0.0135) compared to control. Data are expressed as individual values and as mean±SEM. *: p<0.05; **: p<0.01. ***: p<0.001.

Supplementary Figure 1

(A) Proportion of GLP1-R and GIPR expression in each *Slc32a1*$^{+}$ cluster (B) Number of genes upregulated (red) and downregulated (blue) in response to an overnight fast in each cluster. Genes included were significantly differentially regulated ($P < 0.05$). (C) Top 10 genes differentially expressed in ad libitum vs fasting in *Slc32a1*$^{+}$ neurons (D) Quantification of total NTS c-Fos-expressing cells following 16h fasting and fasting+2h refeeding (n=3, Bregma level: two-way ANOVA $F_{(13,34)}=3.16$; p=0.004; Nutritional state: two-way ANOVA $F_{(1,4)}=18.61$; P=0.012). (E) 12h dark cycle food intake in hM3Dq vs mCherry mice injected with CNO. (F) Food intake following an overnight fast compared to mCherry in GABA^{NTS}:hM3Dq mice (n=6, RM two-way ANOVA $F_{(1,11)}=10.97$; P=0.0069) and (G) 2h food intake (n=6/7, Unpaired t test, $t_{(11)}=3.392$ p=0.006). (G-I) Food intake and body weight change in hM4Di vs mCherry mice twice daily injected with CNO (2mg/Kg). (J-K) Food intake in hM4Di mice co-administered with CNO and Liraglutide (RM: ANOVA $F_{(3,12)}=15.64$; P=0.002, Bonferroni adjusted p=0.0004 Saline vs Liraglutide, P=0.0004 CNO vs Liraglutide and P=0.0263 Liraglutide vs Liraglutide+CNO).

Figure S2. GABA^{NTS} projection pattern and CRACM additional analysis. (A) Representative photomicrographs (scale 100µm) of ChR2-mCherry fibers in a serial rostro-caudal distribution of a *Vgat*^{Cre} mouse brain injected with AAV-DIO-ChR2-mCherry into the NTS. (B-E) A simulated voltage-clamp experiment in an anatomically realistic model of a medium spiny neuron, using the same voltage steps as those described for electrophysiology experiments (Figure 2E-G). The effect of optogenetic stimulation was modelled as a single GABAergic event taking place at each step. (C) Current amplitude was plotted against voltage (as in Figure 2E-G), and a linear fit was used to estimate peak conductance G_s and reversal potential E_{rev}. (D-E) Simulated optogenetic activation of GABA inputs making synaptic contact only on dendrites close to the soma ("prox.", proximal dendrites) was compared to the same type of activation of GABA synapses connected only to dendrites far from the soma ("distal" dendrites) in six different medium spiny neuron models. The reversal potential for GABA in the model was set to -60 mV, and this is close to what was measured at the soma when GABA synaptic inputs were located on dendrites close to the soma. However, when GABA synapses were activated only on dendrites distant from the soma E_{rev}, was more positive than expected and conductance G_s was attenuated. (F) Diagram of

673 outside-out patch technique coupled to a postsynaptic electrical stimulator. (G, left)
674 Representative response of Npy^{hrGFP} cell subjected to series of five electrical stimuli, each
675 evoking excitatory post-synaptic potential (EPSP) of sub-threshold amplitude and (G, right)
676 same cell with electrical stimuli coupled with 470nm light burst. (M) Quantification of receptor
677 opening time (n=5, two-way RM ANOVA $F_{(2,8)}$=11.28; p=0.0047, Bonferroni adjusted
678 P=0.0072 NS vs SL and P=0.0157 S vs SL), L-M n=4-5 cells. (I) Representative response of
679 a single Npy^{hrGFP} cell subjected to 10 series of five electrical stimuli, each evoking excitatory
680 post-synaptic potential (EPSP) of sub-threshold amplitude coupled with 470nm light burst in
681 *Vgat*^{Cre}*::NPY*^{hrGFP} mouse injected with AAV-DIO-ChR2-mCherry into the NTS. NS: No
682 stimulation; S: Stimulation; SL: Stimulation+Light.
683
684

Figure S3. Optogenetic activation of GABA^{NTS}→ARC in *Vgat^{Cre}* mice does not induce anxiety-like behavior. (A) Diagram illustrating open field arena (OFA) task. GABA^{NTS}→ARC does not alter (B) time spent in the center or (C) distance travelled (representative trace of the movement) during the test. (D) Diagram illustrating elevated zero maze (EZM) task. GABA^{NTS}→ARC does not alter (E) time spent in the exposed area or (F) distance travelled in each zone (representative trace of the movement) during the test. (G-H) Quantification of number of interactions with a novel object, a known nutritional food item or a novel palatable food item in mice (G) non-stimulated (RM ANOVA ($F_{(2,10)}$=4.993; p=0.0314, Bonferroni adjusted p=0.0306 NO vs NP) and (H) stimulated (RM ANOVA $F_{(2,10)}$=10.71; p=0.0033, Bonferroni adjusted p=0.0051 NO vs NP; p=0.0121 KN vs NP). Data are expressed as individual values and as mean±S.E.M, n=6 mice. *:p<0.05; **:p<0.01. NO: novel object; NP: novel palatable; KN: known nutritional.

REFERENCES

Aklan, I., Sayar Atasoy, N., Yavuz, Y., Ates, T., Coban, I., Koksalar, F., Filiz, G., Topcu, I. C., Oncul, M., Dilsiz, P., Cebecioglu, U., Alp, M. I., Yilmaz, B., Davis, D. R., Hajdukiewicz, K., Saito, K., Konopka, W., Cui, H., & Atasoy, D. (2020). NTS Catecholamine Neurons Mediate Hypoglycemic Hunger via Medial Hypothalamic Feeding Pathways. *Cell Metabolism*, *31*(2), 313-326.e5. https://doi.org/10.1016/j.cmet.2019.11.016

Alexander, G. M., Rogan, S. C., Abbas, A. I., Armbruster, B. N., Pei, Y., Allen, J. A., Nonneman, R. J., Hartmann, J., Moy, S. S., Nicolelis, M. A., McNamara, J. O., & Roth, B. L. (2009). Remote control of neuronal activity in transgenic mice expressing evolved G protein-coupled receptors. *Neuron*, *63*(1), 27–39. https://doi.org/10.1016/J.NEURON.2009.06.014

Alhadeff, A. L., Mergler, B. D., Zimmer, D. J., Turner, C. A., Reiner, D. J., Schmidt, H. D., Grill, H. J., & Hayes, M. R. (2017). Endogenous Glucagon-like Peptide-1 Receptor Signaling in the Nucleus Tractus Solitarius is Required for Food Intake Control. *Neuropsychopharmacology : Official Publication of the American College of Neuropsychopharmacology*, *42*(7), 1471–1479. https://doi.org/10.1038/NPP.2016.246

Andermann, M. L., & Lowell, B. B. (2017). Toward a Wiring Diagram Understanding of Appetite Control. *Neuron*, *95*(4), 757–778. https://doi.org/10.1016/J.NEURON.2017.06.014

Aponte, Y., Atasoy, D., & Sternson, S. M. (2011). AGRP neurons are sufficient to orchestrate feeding behavior rapidly and without training. *Nature Neuroscience*, *14*(3), 351–355. https://doi.org/10.1038/NN.2739

Berridge, K. C. (2004). Motivation concepts in behavioral neuroscience. *Physiology and Behavior*, *81*(2), 179–209. https://doi.org/10.1016/j.physbeh.2004.02.004

Berrios, J., Li, C., Madara, J. C., Garfield, A. S., Steger, J. S., Krashes, M. J., & Lowell, B. B. (2021). Food cue regulation of AGRP hunger neurons guides learning. *Nature*, *595*, 695. https://doi.org/10.1038/s41586-021-03729-3

Betley, J. N., Cao, Z. F. H., Ritola, K. D., & Sternson, S. M. (2013). Parallel, Redundant Circuit Organization for Homeostatic Control of Feeding Behavior. *Cell*, *155*(6), 1337–1350. https://doi.org/10.1016/J.CELL.2013.11.002

727 Betley, J. N., Xu, S., Cao, Z. F. H., Gong, R., Magnus, C. J., Yu, Y., & Sternson, S. M. (2015).
728 Neurons for hunger and thirst transmit a negative-valence teaching signal. *Nature*,
729 *521*(7551), 180. https://doi.org/10.1038/NATURE14416

730 Blevins, J. E., Schwartz, M. W., & Baskin, D. G. (2004). Evidence that paraventricular nucleus
731 oxytocin neurons link hypothalamic leptin action to caudal brain stem nuclei controlling
732 meal size. *American Journal of Physiology - Regulatory Integrative and Comparative*
733 *Physiology*, *287*(1 56-1), 87–96.
734 https://doi.org/10.1152/AJPREGU.00604.2003/ASSET/IMAGES/LARGE/ZH600704225
735 10005.JPEG

736 Campos, A., Port, J. D., & Acosta, A. (2022). Integrative Hedonic and Homeostatic Food
737 Intake Regulation by the Central Nervous System: Insights from Neuroimaging. In *Brain*
738 *Sciences* (Vol. 12, Issue 4). MDPI. https://doi.org/10.3390/brainsci12040431

739 Chen, H. Y., Trumbauer, M. E., Chen, A. S., Weingarth, D. T., Adams, J. R., Frazier, E. G.,
740 Shen, Z., Marsh, D. J., Feighner, S. D., Guan, X. M., Ye, Z., Nargund, R. P., Smith, R.
741 G., van der Ploeg, L. H. T., Howard, A. D., Macneil, D. J., & Qian, S. (2004). Orexigenic
742 Action of Peripheral Ghrelin Is Mediated by Neuropeptide Y and Agouti-Related Protein.
743 *Endocrinology*, *145*(6), 2607–2612. https://doi.org/10.1210/EN.2003-1596

744 Chen, J., Cheng, M., Wang, L., Zhang, L., Xu, D., Cao, P., Wang, F., Herzog, H., Song, S.,
745 & Zhan, C. (2020). A Vagal-NTS Neural Pathway that Stimulates Feeding. *Current*
746 *Biology*, *30*(20), 3986-3998.e5. https://doi.org/10.1016/J.CUB.2020.07.084

747 Cheng, W., Gordian, D., Ludwig, M. Q., Pers, T. H., Seeley, R. J., & Myers, M. G. (2022).
748 Hindbrain circuits in the control of eating behaviour and energy balance. *Nature*
749 *Metabolism*, *4*(7), 826–835. https://doi.org/10.1038/s42255-022-00606-9

750 Cheng, W., Ndoka, E., Hutch, C., Roelofs, K., MacKinnon, A., Khoury, B., Magrisso, J., Kim,
751 K. S., Rhodes, C. J., Olson, D. P., Seeley, R. J., Sandoval, D., & Myers, M. G. (2020).
752 Leptin receptor-expressing nucleus tractus solitarius neurons suppress food intake
753 independently of GLP1 in mice. *JCI Insight*, *5*(7).
754 https://doi.org/10.1172/JCI.INSIGHT.134359

755 Clifton, P. G. (2000). Meal patterning in rodents: psychopharmacological and
756 neuroanatomical studies. *Neuroscience & Biobehavioral Reviews*, *24*(2), 213–222.
757 https://doi.org/10.1016/S0149-7634(99)00074-3

758 Cork, S. C., Richards, J. E., Holt, M. K., Gribble, F. M., Reimann, F., & Trapp, S. (2015).
759 Distribution and characterisation of Glucagon-like peptide-1 receptor expressing cells in
760 the mouse brain. *Molecular Metabolism*, *4*(10), 718–731.
761 https://doi.org/10.1016/j.molmet.2015.07.008

762 Cummings, D. E., Purnell, J. Q., Frayo, R. S., Schmidova, K., Wisse, B. E., & Weigle, D. S.
763 (2001). A Preprandial Rise in Plasma Ghrelin Levels Suggests a Role in Meal Initiation
764 in Humans. *Diabetes*, *50*(8), 1714–1719. https://doi.org/10.2337/DIABETES.50.8.1714

765 D'Agostino, G., & Luckman, S. M. (2022). Brainstem peptides and peptidergic neurons in the
766 regulation of appetite. *Current Opinion in Endocrine and Metabolic Research*, *24*,
767 100339. https://doi.org/10.1016/J.COEMR.2022.100339

768 D'Agostino, G., Lyons, D., Cristiano, C., Lettieri, M., Olarte-Sanchez, C., Burke, L. K.,
769 Greenwald-Yarnell, M., Cansell, C., Doslikova, B., Georgescu, T., Martinez de Morentin,
770 P. B., Myers, M. G., Rochford, J. J., & Heisler, L. K. (2018). Nucleus of the Solitary Tract
771 Serotonin 5-HT2C Receptors Modulate Food Intake. *Cell Metabolism*, *28*(4), 619-
772 630.e5. https://doi.org/10.1016/J.CMET.2018.07.017

773 D'Agostino, G., Lyons, D. J., Cristiano, C., Burke, L. K., Madara, J. C., Campbell, J. N.,
774 Garcia, A. P., Land, B. B., Lowell, B. B., Dileone, R. J., & Heisler, L. K. (2016). Appetite
775 controlled by a cholecystokinin nucleus of the solitary tract to hypothalamus neurocircuit.
776 *ELife*, *5*. https://doi.org/10.7554/eLife.12225

777 Deem, J. D., Faber, C. L., & Morton, G. J. (2022). AgRP neurons: Regulators of feeding,
778 energy expenditure, and behavior. *FEBS Journal*, *289*(8), 2362–2381.
779 https://doi.org/10.1111/FEBS.16176

780 Dietrich, M. O., Bober, J., Ferreira, J. G., Tellez, L. A., Mineur, Y. S., Souza, D. O., Gao, X.-
781 B., Picciotto, M. R., Araújo, I., Liu, Z.-W., & Horvath, T. L. (2012). AgRP neurons regulate
782 development of dopamine neuronal plasticity and nonfood-associated behaviors. *Nature*
783 *Neuroscience*. https://doi.org/10.1038/nn.3147

784 Dietrich, M. O., Zimmer, M. R., Bober, J., & Horvath, T. L. (2015). Hypothalamic Agrp Neurons
785 Drive Stereotypic Behaviors beyond Feeding. *Cell*, *160*(6), 1222–1232.
786 https://doi.org/10.1016/J.CELL.2015.02.024

787 Dowsett, G. K. C., Lam, B. Y. H., Tadross, J. A., Cimino, I., Rimmington, D., Coll, A. P., Polex-
788 Wolf, J., Knudsen, L. B., Pyke, C., & Yeo, G. S. H. (2021). A survey of the mouse
789 hindbrain in the fed and fasted states using single-nucleus RNA sequencing. *Molecular*
790 *Metabolism*, *53*, 101240. https://doi.org/10.1016/J.MOLMET.2021.101240

791 Fenno, L. E., Mattis, J., Ramakrishnan, C., & Deisseroth, K. (2017). A Guide to Creating and
792 Testing New INTRSECT Constructs. *Current Protocols in Neuroscience*, *80*(1), 4.39.1-
793 4.39.24. https://doi.org/10.1002/CPNS.30

794 Fenno, L. E., Mattis, J., Ramakrishnan, C., Hyun, M., Lee, S. Y., He, M., Tucciarone, J.,
795 Selimbeyoglu, A., Berndt, A., Grosenick, L., Zalocusky, K. A., Bernstein, H., Swanson,
796 H., Perry, C., Diester, I., Boyce, F. M., Bass, C. E., Neve, R., Huang, Z. J., & Deisseroth,
797 K. (2014). Targeting cells with single vectors using multiple-feature Boolean logic. *Nature*
798 *Methods*, *11*(7), 763–772. https://doi.org/10.1038/nmeth.2996

799 Fortin, S. M., Lipsky, R. K., Lhamo, R., Chen, J., Kim, E., Borner, T., Schmidt, H. D., & Hayes,
800 M. R. (2020). GABA neurons in the nucleus tractus solitarius express GLP-1 receptors
801 and mediate anorectic effects of liraglutide in rats HHS Public Access. *Sci Transl Med*,
802 *12*(533), 109–114. https://doi.org/10.1126/scitranslmed.aay8071

803 Garau, C., Blomeley, C., Burdakov, D., & Burdakov, D. (2020). Orexin neurons and inhibitory
804 Agrp→orexin circuits guide spatial exploration in mice. *The Journal of Physiology*, *598*,
805 4371–4383. https://doi.org/10.1113/JP280158

806 Georgescu, T., Lyons, D., Doslikova, B., Garcia, A. P., Marston, O., Burke, L. K., Chianese,
807 R., Lam, B. Y. H., Yeo, G. S. H., Rochford, J. J., Garfield, A. S., & Heisler, L. K. (2020).
808 Neurochemical Characterization of Brainstem Pro-Opiomelanocortin Cells.
809 *Endocrinology*, *161*(4). https://doi.org/10.1210/endocr/bqaa032

810 González, J. A., Iordanidou, P., Strom, M., Adamantidis, A., & Burdakov, D. (2016). Awake
811 dynamics and brain-wide direct inputs of hypothalamic MCH and orexin networks. *Nature*
812 *Communications*, *7*. https://doi.org/10.1038/NCOMMS11395

813 Graham, D. L., Durai, H. H., Trammell, T. S., Noble, B. L., Mortlock, D. P., Galli, A., &
814 Stanwood, G. D. (2020). A novel mouse model of glucagon-like peptide-1 receptor
815 expression: A look at the brain. *Journal of Comparative Neurology*, *528*(14), 2445–2470.
816 https://doi.org/10.1002/cne.24905

817 Grill, H. J., & Hayes, M. R. (2012). Hindbrain Neurons as an Essential Hub in the
818 Neuroanatomically Distributed Control of Energy Balance. *Cell Metabolism*, *16*(3), 296–
819 309. https://doi.org/10.1016/J.CMET.2012.06.015

820 Hahn, T. M., Breininger, J. F., Baskin, D. G., & Schwartz, M. W. (1998). Coexpression of Agrp
821 and NPY in fasting-activated hypothalamic neurons. *Nature Neuroscience 1998 1:4*,
822 *1*(4), 271–272. https://doi.org/10.1038/1082

823 Han, Y., Xia, G., Srisai, D., Meng, F., He, Y., Ran, Y., He, Y., Farias, M., Hoang, G., Tóth, I.,
824 Dietrich, M. O., Chen, M. H., Xu, Y., & Wu, Q. (2021). Deciphering an AgRP-
825 serotoninergic neural circuit in distinct control of energy metabolism from feeding. *Nature*
826 *Communications 2021 12:1*, *12*(1), 1–16. https://doi.org/10.1038/s41467-021-23846-x

827 Hao, Y., Hao, S., Andersen-Nissen, E., Mauck, W. M., Zheng, S., Butler, A., Lee, M. J., Wilk,
828 A. J., Darby, C., Zager, M., Hoffman, P., Stoeckius, M., Papalexi, E., Mimitou, E. P., Jain,
829 J., Srivastava, A., Stuart, T., Fleming, L. M., Yeung, B., … Satija, R. (2021). Integrated
830 analysis of multimodal single-cell data. *Cell*, *184*(13), 3573-3587.e29.
831 https://doi.org/10.1016/j.cell.2021.04.048

832 Heinz, D. E., Schöttle, V. A., Nemcova, P., Binder, F. P., Ebert, T., Domschke, K., & Wotjak,
833 C. T. (2021). Exploratory drive, fear, and anxiety are dissociable and independent
834 components in foraging mice. *Translational Psychiatry 2021 11:1*, *11*(1), 1–12.
835 https://doi.org/10.1038/s41398-021-01458-9

836 Heisler, L. K., Jobst, E. E., Sutton, G. M., Zhou, L., Borok, E., Thornton-Jones, Z., Liu, H. Y.,
837 Zigman, J. M., Balthasar, N., Kishi, T., Lee, C. E., Aschkenasi, C. J., Zhang, C. Y., Yu,
838 J., Boss, O., Mountjoy, K. G., Clifton, P. G., Lowell, B. B., Friedman, J. M., … Cowley,
839 M. A. (2006). Serotonin Reciprocally Regulates Melanocortin Neurons to Modulate Food
840 Intake. *Neuron*, *51*(2), 239–249. https://doi.org/10.1016/j.neuron.2006.06.004

841 Heisler, L. K., & Lam, D. D. (2017). An appetite for life: brain regulation of hunger and satiety.
842 *Current Opinion in Pharmacology*, *37*, 100–106.
843 https://doi.org/10.1016/J.COPH.2017.09.002

844 Hentges, S. T., Otero-Corchon, V., Pennock, R. L., King, C. M., & Low, M. J. (2009).
845 Proopiomelanocortin Expression in both GABA and Glutamate Neurons. *The Journal of*
846 *Neuroscience*, *29*(43), 13684–13690. https://doi.org/10.1523/JNEUROSCI.3770-
847 09.2009

Holt, M. K., Richards, J. E., Cook, D. R., Brierley, D. I., Williams, D. L., Reimann, F., Gribble, F. M., & Trapp, S. (2019). Preproglucagon neurons in the nucleus of the solitary tract are the main source of brain GLP-1, mediate stress-induced hypophagia, and limit unusually large intakes of food. *Diabetes*, *68*(1), 21–33. https://doi.org/10.2337/DB18-0729/-/DC1

Hyun, U., & Sohn, J. W. (2022). Autonomic control of energy balance and glucose homeostasis. *Experimental & Molecular Medicine 2022 54:4*, *54*(4), 370–376. https://doi.org/10.1038/s12276-021-00705-9

Jensen, C. B., Pyke, C., Rasch, M. G., Dahl, A. B., Knudsen, L. B., & Secher, A. (2018). Characterization of the Glucagonlike Peptide-1 Receptor in Male Mouse Brain Using a Novel Antibody and In Situ Hybridization. *Endocrinology*, *159*(2), 665–675. https://doi.org/10.1210/en.2017-00812

Jikomes, N., Ramesh, R. N., Mandelblat-Cerf, Y., & Andermann, M. L. (2016). Preemptive Stimulation of AgRP Neurons in Fed Mice Enables Conditioned Food Seeking under Threat. *Current Biology*, *26*(18), 2500–2507. https://doi.org/10.1016/J.CUB.2016.07.019

Kim, S. Y., Adhikari, A., Lee, S. Y., Marshel, J. H., Kim, C. K., Mallory, C. S., Lo, M., Pak, S., Mattis, J., Lim, B. K., Malenka, R. C., Warden, M. R., Neve, R., Tye, K. M., & Deisseroth, K. (2013). Diverging neural pathways assemble a behavioural state from separable features in anxiety. *Nature 2013 496:7444*, *496*(7444), 219–223. https://doi.org/10.1038/nature12018

Krashes, M. J., Koda, S., Ye, C. P., Rogan, S. C., Adams, A. C., Cusher, D. S., Maratos-Flier, E., Roth, B. L., & Lowell, B. B. (2011). Rapid, reversible activation of AgRP neurons drives feeding behavior in mice. *Journal of Clinical Investigation*, *121*(4), 1424–1428. https://doi.org/10.1172/JCI46229

Krashes, M. J., Shah, B. P., Madara, J. C., Olson, D. P., Strochlic, D. E., Garfield, A. S., Vong, L., Pei, H., Watabe-Uchida, M., Uchida, N., Liberles, S. D., & Lowell, B. B. (2014). An excitatory paraventricular nucleus to AgRP neuron circuit that drives hunger. *Nature 2014 507:7491*, *507*(7491), 238–242. https://doi.org/10.1038/nature12956

Krnjević, K., & Schwartz, S. (1967). The action of γ-Aminobutyric acid on cortical neurones. *Experimental Brain Research*, *3*(4), 320–336. https://doi.org/10.1007/BF00237558

877 Li, C., Hou, Y., Zhang, J., Sui, G., Du, X., Licinio, J., Wong, M. L., & Yang, Y. (2019). AGRP
878 neurons modulate fasting-induced anxiolytic effects. *Translational Psychiatry 2019 9:1*,
879 *9*(1), 1–10. https://doi.org/10.1038/s41398-019-0438-1

880 Lin, J. Y., Lin, M. Z., Steinbach, P., & Tsien, R. Y. (2009). Characterization of Engineered
881 Channelrhodopsin Variants with Improved Properties and Kinetics. *Biophysical Journal*,
882 *96*(5), 1803–1814. https://doi.org/10.1016/J.BPJ.2008.11.034

883 Lindroos, R., & Hellgren Kotaleski, J. (2021). Predicting complex spikes in striatal projection
884 neurons of the direct pathway following neuromodulation by acetylcholine and dopamine.
885 *The European Journal of Neuroscience*, *53*(7), 2117–2134.
886 https://doi.org/10.1111/ejn.14891

887 Liu, J., Conde, K., Zhang, P., Lilascharoen, V., Xu, Z., Lim, B. K., Seeley, R. J., Zhu, J. J.,
888 Scott, M. M., & Pang, Z. P. (2017). Enhanced AMPA receptor trafficking mediates the
889 anorexigenic effect of endogenous glucagon like peptide-1 in the paraventricular
890 hypothalamus. *Neuron*, *96*(4), 897. https://doi.org/10.1016/J.NEURON.2017.09.042

891 Ludwig, M. Q., Cheng, W., Gordian, D., Lee, J., Paulsen, S. J., Hansen, S. N., Egerod, K. L.,
892 Barkholt, P., Rhodes, C. J., Secher, A., Knudsen, L. B., Pyke, C., Myers, M. G., & Pers,
893 T. H. (2021). A genetic map of the mouse dorsal vagal complex and its role in obesity.
894 *Nature Metabolism*, *3*(4), 530–545. https://doi.org/10.1038/s42255-021-00363-1

895 Luquet, S., Perez, F. A., Hnasko, T. S., & Palmiter, R. D. (2005). NPY/AgRP neurons are
896 essentials for feeding in adult mice but can be ablated in neonates. *Science*, *310*(5748),
897 683–685. https://doi.org/10.1126/SCIENCE.1115524

898 Luquet, S., Phillips, C. T., & Palmiter, R. D. (2007). NPY/AgRP neurons are not essential for
899 feeding responses to glucoprivation. *Peptides*, *28*(2), 214–225.
900 https://doi.org/10.1016/J.PEPTIDES.2006.08.036

901 Madisen, L., Zwingman, T. A., Sunkin, S. M., Oh, S. W., Zariwala, H. A., Gu, H., Ng, L. L.,
902 Palmiter, R. D., Hawrylycz, M. J., Jones, A. R., Lein, E. S., & Zeng, H. (2009). A robust
903 and high-throughput Cre reporting and characterization system for the whole mouse
904 brain. *Nature Neuroscience 2009 13:1*, *13*(1), 133–140. https://doi.org/10.1038/nn.2467

905 Mandelblat-Cerf, Y., Ramesh, R. N., Burgess, C. R., Patella, P., Yang, Z., Lowell, B. B., &
906 Andermann, M. L. (2015). Arcuate hypothalamic AgRP and putative POMC neurons

907 show opposite changes in spiking across multiple timescales. *ELife*, *4*.
908 https://doi.org/10.7554/eLife.07122

909 Olson, B. R., Freilino, M., Hoffman, G. E., Stricker, E. M., Sved, A. F., & Verbalis, J. G. (1993).
910 C-Fos expression in rat brain and brainstem nuclei in response to treatments that alter
911 food intake and gastric motility. *Molecular and Cellular Neurosciences*, *4*(1), 93–106.
912 https://doi.org/10.1006/MCNE.1993.1011

913 Petreanu, L., Huber, D., Sobczyk, A., & Svoboda, K. (2007). *Channelrhodopsin-2-assisted*
914 *circuit mapping of long-range callosal projections*. https://doi.org/10.1038/nn1891

915 Richard, C. D., Tolle, V., & Low, M. J. (2011). Meal pattern analysis in neural-specific
916 proopiomelanocortin-deficient mice. *European Journal of Pharmacology*, *660*(1), 131–
917 138. https://doi.org/10.1016/J.EJPHAR.2010.12.022

918 Shi, M. Y., Ding, L. F., Guo, Y. H., Cheng, Y. X., Bi, G. Q., & Lau, P. M. (2021). Long-range
919 GABAergic projections from the nucleus of the solitary tract. *Molecular Brain*, *14*(1), 1–
920 5. https://doi.org/10.1186/S13041-021-00751-4/FIGURES/1

921 Spruston, N., Jaffe, D. B., Williams, S. H., & Johnston, D. (1993). Voltage- and space-clamp
922 errors associated with the measurement of electrotonically remote synaptic events.
923 *Journal of Neurophysiology*, *70*(2), 781–802. https://doi.org/10.1152/jn.1993.70.2.781

924 Stamatakis, A. M., & Stuber, G. D. (2012). Activation of lateral habenula inputs to the ventral
925 midbrain promotes behavioral avoidance. *Nature Neuroscience 2012 15:8*, *15*(8), 1105–
926 1107. https://doi.org/10.1038/nn.3145

927 Sylantyev, S., Savtchenko, L. P., O'Neill, N., & Rusakov, D. A. (2020). Extracellular GABA
928 waves regulate coincidence detection in excitatory circuits. *The Journal of Physiology*,
929 *598*(18), 4047. https://doi.org/10.1113/JP279744

930 Tsang, A. H., Nuzzaci, D., Darwish, T., Samudrala, H., & Blouet, C. (2020). Nutrient sensing
931 in the nucleus of the solitary tract mediates non-aversive suppression of feeding via
932 inhibition of AgRP neurons. *Molecular Metabolism*, *42*, 101070.
933 https://doi.org/10.1016/J.MOLMET.2020.101070

934 van den Pol, A. N., Yao, Y., Fu, L. Y., Foo, K., Huang, H., Coppari, R., Lowell, B. B., &
935 Broberger, C. (2009). Neuromedin B and gastrin-releasing peptide excite arcuate
936 nucleus neuropeptide Y neurons in a novel transgenic mouse expressing strong Renilla

937 green fluorescent protein in NPY neurons. *The Journal of Neuroscience : The Official*
938 *Journal of the Society for Neuroscience*, *29*(14), 4622–4639.
939 https://doi.org/10.1523/JNEUROSCI.3249-08.2009

940 Vong, L., Ye, C., Yang, Z., Choi, B., Chua, S., & Lowell, B. B. (2011). Leptin action on
941 GABAergic neurons prevents obesity and reduces inhibitory tone to POMC neurons.
942 *Neuron*, *71*(1), 142–154. https://doi.org/10.1016/J.NEURON.2011.05.028

943 Wagner, S., Brierley, D. I., Leeson-Payne, A., Jiang, W., Chianese, R., Lam, B. Y. H.,
944 Dowsett, G. K. C., Cristiano, C., Lyons, D., Reimann, F., Gribble, F. M., Martinez de
945 Morentin, P. B., Yeo, G. S. H., Trapp, S., & Heisler, L. K. (2022). Obesity medication
946 lorcaserin activates brainstem GLP-1 neurons to reduce food intake and augments GLP-
947 1 receptor agonist induced appetite suppression. *Molecular Metabolism*, *68*.
948 https://doi.org/10.1016/J.MOLMET.2022.101665

949 Wang, C., Zhou, W., He, Y., Yang, T., Xu, P., Yang, Y., Cai, X., Wang, J., Liu, H., Yu, M.,
950 Liang, C., Yang, T., Liu, H., Fukuda, M., Tong, Q., Wu, Q., Sun, Z., He, Y., & Xu, Y.
951 (2021). AgRP neurons trigger long-term potentiation and facilitate food seeking.
952 *Translational Psychiatry*, *11*, 11. https://doi.org/10.1038/s41398-020-01161-1

953 Williams, D. L., & Schwartz, M. W. (2005). The melanocortin system as a central integrator
954 of direct and indirect controls of food intake. *American Journal of Physiology. Regulatory,*
955 *Integrative and Comparative Physiology*, *289*(1).
956 https://doi.org/10.1152/AJPREGU.00226.2005

957 Wu, Q., Lemus, M. B., Stark, R., Bayliss, J. A., Reichenbach, A., Lockie, S. H., & Andrews,
958 Z. B. (2014). The Temporal Pattern of cfos Activation in Hypothalamic, Cortical, and
959 Brainstem Nuclei in Response to Fasting and Refeeding in Male Mice. *Endocrinology*,
960 *155*(3), 840–853. https://doi.org/10.1210/EN.2013-1831

961 Yavari, A., Stocker, C. J., Ghaffari, S., Wargent, E. T., Steeples, V., Czibik, G., Pinter, K.,
962 Bellahcene, M., Woods, A., Martinez de Morentin, P. B., Cansell, C., Lam, B. Y., Chuster,
963 A., Petkevicius, K., Nguyen-Tu, M. S., Martinez-Sanchez, A., Pullen, T. J., Oliver, P. L.,
964 Stockenhuber, A., … Ashrafian, H. (2016). Chronic Activation of gamma2 AMPK Induces
965 Obesity and Reduces beta Cell Function. *Cell Metab*, *23*(5), 821–836.
966 https://doi.org/10.1016/j.cmet.2016.04.003

967 Zhan, C., Zhou, J., Feng, Q., Zhang, J. en, Lin, S., Bao, J., Wu, P., & Luo, M. (2013). Acute
968 and long-term suppression of feeding behavior by POMC neurons in the brainstem and
969 hypothalamus, respectively. *The Journal of Neuroscience : The Official Journal of the*
970 *Society for Neuroscience*, *33*(8), 3624–3632.
971 https://doi.org/10.1523/JNEUROSCI.2742-12.2013

972 Zingg, B., Chou, X. lin, Zhang, Z. gang, Mesik, L., Liang, F., Tao, H. W., & Zhang, L. I. (2017).
973 AAV-Mediated Anterograde Transsynaptic Tagging: Mapping Corticocollicular Input-
974 Defined Neural Pathways for Defense Behaviors. *Neuron*, *93*(1), 33–47.
975 https://doi.org/10.1016/J.NEURON.2016.11.045

976 Zorrilla, E. P., Inoue, K., Fekete, É. M., Tabarin, A., Valdez, G. R., & Koob, G. F. (2005).
977 Measuring meals: Structure of prandial food and water intake of rats. *American Journal*
978 *of Physiology - Regulatory Integrative and Comparative Physiology*, *288*(6 57-6), 1450–
979 1467.
980 https://doi.org/10.1152/AJPREGU.00175.2004/SUPPL_FILE/ZORRILLA_SUPP_TABL
981 E.PDF

982